Lunar laser ranging constraints on nonminimally coupled dark energy and standard sirens

Shinji Tsujikawa

Department of Physics, Faculty of Science, Tokyo University of Science, 1-3, Kagurazaka, Shinjuku-ku, Tokyo 162-8601, Japan

(Received 17 March 2019; published 6 August 2019)

In dark energy models where a scalar field ϕ is coupled to the Ricci scalar R of the form $e^{-2Q(\phi-\phi_0)/M_{\rm pl}}R$, where Q is a coupling constant, ϕ_0 is today's value of ϕ, and $M_{\rm pl}$ is the reduced Planck mass, we study how the recent Lunar Laser Ranging (LLR) experiment places constraints on the nonminimal coupling from the time variation of gravitational coupling. Besides a potential of the light scalar responsible for cosmic acceleration, we take a cubic Galileon term into account to suppress fifth forces in overdensity regions of the Universe. Even if the scalar-matter interaction is screened by the Vainshtein mechanism, the time variation of gravitational coupling induced by the cosmological background field ϕ survives in the solar system. For a small Galileon coupling constant β_3, there exists a kinetically driven ϕ-matter-dominated-epoch (ϕMDE) prior to cosmic acceleration. In this case, we obtain the stringent upper limit $Q \leq 3.4 \times 10^{-3}$ from the LLR constraint. For a large β_3 without the ϕMDE, the coupling Q is not particularly bounded from above, but the cosmological Vainshtein screening strongly suppresses the time variation of ϕ such that the dark energy equation of state $w_{\rm DE}$ reaches the value close to -1 at high redshifts. We study the modified gravitational wave propagation induced by the nonminimal coupling to gravity and show that, under the LLR bound, the difference between the gravitational wave and luminosity distances does not exceed the order 10^{-5} over the redshift range $0 < z < 100$. In dark energy models where the Vainshtein mechanism is at work through scalar derivative self-interactions, it is difficult to probe the signature of nonminimal couplings from the observations of standard sirens.

DOI: 10.1103/PhysRevD.100.043510

I. INTRODUCTION

Since the first discovery of late-time cosmic acceleration by supernovae type Ia (SN Ia) in 1998 [1,2], the origin of this phenomenon has not yet been identified. A scalar field ϕ is one of the simplest candidates for dark energy, whose potential energy [3] or nonlinear kinetic energy [4] can drive the acceleration. If we allow for the coupling between ϕ and the gravity sector, Horndeski theories [5] are known as the most general scalar-tensor theories with second-order equations of motion [6–8].

Dark energy models based on Horndeski theories can be constrained not only by the observational data of SNIa, cosmic microwave background (CMB) temperature anisotropies, and baryon acoustic cscillations (BAO) but also by the measurements of gravitational waves (GWs). The bound on the speed of GWs from gravitational Cherenkov radiation [9] was used in Ref. [10] to place constraints on the Lagrangian of Horndeski theories. After the first discovery of the GW event GW150914 [11], the possibility for constraining modified gravity models from the measurements of GWs along with gamma-ray bursts was pointed out in Ref. [12]. From the Hulse-Taylor pulsar data, the speed of GWs c_t was also constrained to be close to that of light c at the level of 10^{-2} [13].

The GW170817 event from a neutron star merger [14] together with electromagnetic counterparts [15] showed that the relative difference between c_t and c is less than the order 10^{-15}. If we strictly demand that $c_t = c$ on the isotropic cosmological background, the allowed Horndeski Lagrangian is of the form $L = G_2(\phi, X) + G_3(\phi, X)\Box\phi + G_4(\phi)R$, where G_2 and G_3 are functions of ϕ and $X = -\partial_\mu\phi\partial^\mu\phi/2$, while G_4 is a function of ϕ alone [16–20]. This includes the theories such as quintessence [3], k-essence [4], cubic Galileons [21–24], Brans-Dicke (BD) theory [25], $f(R)$ gravity [26–28], and nonminimally coupled theories with general functions $G_4(\phi)$ [29–38].

The original massless BD theory [25] is equivalent to the Lagrangian $L = (1-6Q^2)F(\phi)X + (M_{\rm pl}^2/2)F(\phi)R$ with $F(\phi) = e^{-2Q(\phi-\phi_0)/M_{\rm pl}}$, where the constant Q is related to the so-called BD parameter $\omega_{\rm BD}$, as $2Q^2 = 1/(3+2\omega_{\rm BD})$ [38]. General relativity (GR) is recovered in the limit $\omega_{\rm BD} \to \infty$, i.e., $Q \to 0$. If we transform the action of BD theory to that in the Einstein frame, the constant Q has a meaning of coupling between the scalar field and nonrelativistic matter [39].

The parametrized post-Newtonian (PPN) formalism [40,41] on the weak gravitational background shows that,

in massless BD theory, one of the PPN parameters is given by $\gamma = (1+\omega_{\rm BD})/(2+\omega_{\rm BD})$ [42]. The Cassini experiment measuring the time delay of light in the solar system placed the constraint $|\gamma - 1| \le 2.3 \times 10^{-5}$ [43]. This translates to the bound $\omega_{\rm BD} \ge 4.3 \times 10^4$ or, equivalently, $|Q| \le 2.4 \times 10^{-3}$. For the coupling $|Q| > 2.4 \times 10^{-3}$, one needs to resort to some mechanism for screening fifth forces mediated by the BD scalar field.

If the BD scalar has a massive potential in overdensity regions of the Universe, the propagation of fifth forces can be suppressed under the chameleon mechanism [44,45]. For example, metric $f(R)$ gravity corresponds to BD theory with $Q = -1/\sqrt{6}$ in the presence of a scalar potential of gravitational origin [39,46]. It is possible to design the form of $f(R)$ such that the scalar degree of freedom (scalaron) has a heavy mass in overdensity regions, while realizing cosmic acceleration by a light scalar on Hubble scales [47–50]. However, this amounts to a fine-tuning of initial conditions of scalaron perturbations in the early universe [48,50,51]. Moreover, unless the scalaron is nearly frozen until recently, the large coupling $|Q| \simeq 0.4$ leads to the significant enhancement of matter perturbations in the late universe [47,48,50,52,53]. For the compatibility of $f(R)$ models of late-time cosmic acceleration with observations, the deviation from GR is required to be very small, and hence they are hardly distinguishable from the Λ-cold-dark-matter (ΛCDM) model [54,55].

There is yet another mechanism for screening fifth forces in local regions of the Universe based on nonlinear derivative self-interactions [56]. A representative example is the cubic Galileon Lagrangian $X\Box\phi$ [21–24], with which the Newtonian behavior is recovered inside the so-called Vainshtein radius r_V [57–65] even with the coupling $|Q| > 2.4 \times 10^{-3}$. For uncoupled Galileons ($Q = 0$) without the scalar potential, it is known that there exists a cosmological tracker solution finally approaching a de Sitter attractor [66,67] (see also Refs. [68,69]). Unfortunately, this dark energy model is in tension with the observational data of supernovae type Ia, CMB, BAO, and redshift-space distortions [70–76]. For the nonminimally coupled light mass or massless Galileon with a potential, e.g., the linear potential $V(\phi) = m^3\phi$, it is possible to realize the viable cosmic expansion history, while recovering the Newtonian behavior in the solar system [77,78].

While the Vainshtein mechanism suppresses the scalar-matter interaction for the distance $r \ll r_V$, the gravitational coupling $G_{\rm N}$ in overdensity regions contains time dependence of the dark energy field ϕ through the nonminimal coupling $F(\phi)$ [62,64]. Then, $G_{\rm N}$ varies in time even inside the solar system. The Lunar Laser Ranging (LLR) experiments of the earth-moon system measure the time variation $\dot{G}_{\rm N}/G_{\rm N}$, so it can be used to constrain nonminimally coupled dark energy models.

From the LLR bound of $\dot{G}_{\rm N}/G_{\rm N}$ in 2004 [79], the time variation $\alpha_{\rm M} \equiv \dot{F}/(HF)$ (where H is the Hubble expansion rate) is in the range $|\alpha_{\rm M}(t_0)| \le 0.02$ today. In 2011, Babichev *et al.* [62] used this bound for nonminimally coupled cubic Galileons without the potential and claimed that the time variation of the field is tightly constrained at low redshifts. We note that, besides this fact, the cubic Galileon without the potential is in tension with the observational data. On the other hand, the presence of potentials for nonminimally coupled Galileons allows the possibility for realizing viable cosmic expansion and growth histories, even with the LLR bound in 2004; see Figs. 4 and 5 in Ref. [80].

The recent LLR experiments [81] constrain the time variation $\dot{G}_{\rm N}/G_{\rm N}$ with the upper limit more stringent than before [79]. In particular, for $\alpha_{\rm M} > 0$, the upper bound of $\dot{G}_{\rm N}/G_{\rm N}$ translates to $\alpha_{\rm M}(t_0) \le 7 \times 10^{-5}$ today, which is tighter than the bound $\alpha_{\rm M}(t_0) \le 0.02$ by more than 2 orders of magnitude. This LLR bound in 2018 was used to constrain dark energy models based on nonlocal gravity [82]. It remains to be seen how nonminimally coupled Galileons with the potential can be constrained with this new bound of $\alpha_{\rm M}(t_0)$.

In this paper, we exploit the new LLR bound to constrain nonminimally coupled dark energy models with the cubic self-interaction $\beta_3 M^{-3} X\Box\phi$ and the potential $V(\phi)$ of light mass Galileons, where β_3 is a dimensionless coupling constant and M is a mass scale defined later in Eq. (2.2). We stress that our model is different from the nonminimally coupled cubic Galileon without the potential studied in Ref. [62], in that the scalar potential is the dominant source for late-time cosmic acceleration. The Galileon term can still play an important role for the scalar field dynamics in the early universe. Moreover, we require that the propagation of fifth forces is suppressed in overdensity regions. We perform a detailed analysis for the cosmological dynamics from the radiation era to today and put bounds on the coupling Q by using the new LLR data.

For $|\beta_3| \ll 1$, there exists a so-called ϕ-matter-dominated epoch (ϕMDE) [83] in the Jordan frame followed by the stage of cosmic acceleration. For the exponential potential $V(\phi) = V_0 e^{\lambda\phi/M_{\rm pl}}$, we place constraints on the allowed parameter space in the (λ, Q) plane and derive the stringent limit $Q \le 3.4 \times 10^{-3}$ from the LLR constraint. This is almost close to the Cassini bound $Q \le 2.4 \times 10^{-3}$ obtained for massless BD theories without the Vainshtein screening. For $|\beta_3| \gg 1$, the coupling Q is not particularly bounded from above due to the suppression of field kinetic energy under the cosmological Vainshtein screening. In this case, we show a new possibility for realizing the dark energy equation of state $w_{\rm DE}$ close to -1 from high redshifts to today even for the steep potential satisfying $\lambda > \sqrt{2}$.

In our dark energy theory the speed of GWs is equivalent to that of light, but the existence of nonminimal coupling $F(\phi)$ leads to the modified GW propagation through the existence of a nonvanishing term $\alpha_{\rm M}$. The possibility of using the difference between GW and luminosity distances

to test for the running Planck mass was first pointed out in Ref. [84]. The first forecasts of such constraints were given in Ref. [12], which were followed by a sequence of papers after the direct detection of GWs [85–92].

In Ref. [12], it was anticipated that the LLR bound on the running Planck mass may be beyond the reach of the constraint arising from standard sirens. This generally depends on the models of dark energy. For example, in nonlocal gravity models studied recently in Ref. [82], the difference between the GW distance $d_{\rm GW}$ and luminosity distance d_L is typically more than a few percent, which may be probed in future high-precision measurements. This reflects the fact that, in nonlocal gravity, the gravitational coupling deep inside the Hubble radius (wavelength $a/k \ll H^{-1}$) is very close to the Newton gravitational constant G, as $G_{\rm N}/G = 1 + \mathcal{O}((aH/k)^2)$ [82,93]. Hence the nonlocal gravity models can pass the new LLR bound in 2018, while leaving the sizable difference between $d_{\rm GW}$ and d_L.

The nonminimal coupling $G_4(\phi)R$ gives rise to the effective gravitational coupling $G_{\rm N}$ different from that in nonlocal gravity. Hence it deserves to be studied whether the new LLR data leads to the constraint on the nonminimal coupling beyond or within the reach of future standard siren measurements. In this paper, we will compute the relative ratio between $d_{\rm GW}$ and d_L for the aforementioned nonminimally coupled dark energy model. Under the LLR bound on the variation of $F(\phi)$, we show that the relative difference $d_{\rm GW}/d_L - 1$ does not exceed the order 10^{-5} in the redshift range $0 < z < 100$. Thus, unlike nonlocal gravity, the LLR data allow only tiny deviations of $d_{\rm GW}$ from d_L in nonminimally coupled theories, so it will be difficult to detect such a difference without very high-precision distance measurements in the future.

This paper is organized as follows. In Sec. II, we present our nonminimally coupled dark energy model and revisit how the cubic Galileon interaction screens the scalar-matter coupling under the Vainshtein mechanism. We then interpret the recent LLR bound in terms of today's value of $\alpha_{\rm M}$. In Sec. III, we derive the background equations of motion on the flat Friedmann-Lemaître-Robertson-Walker (FLRW) background and express them in autonomous forms. In Sec. IV, we study the cosmological dynamics in the presence of exponential potential $V(\phi) = V_0 e^{\lambda\phi/M_{\rm pl}}$ for unscreened ($|\beta_3| \ll 1$) and screened ($|\beta_3| \gg 1$) cases after the radiation domination. We put constraints on the allowed parameter space from the recent LLR bound and discuss the evolution of $w_{\rm DE}$ and field density parameters. In Sec. V, we investigate how much difference arises between $d_{\rm GW}(z)$ and $d_L(z)$ for the two different background cosmologies discussed in Sec. IV. Section VI is devoted to conclusions.

Unless otherwise stated, we use the natural unit where the speed of light c, the reduced Planck constant $\hbar$, and the Boltzmann constant k_B are equivalent to 1.

II. NONMINIMALLY COUPLED THEORIES AND LLR CONSTRAINTS

We begin with a subclass of Horndeski theories given by the action

$$\mathcal{S} = \int {\rm d}^4x\sqrt{-g}\left[\frac{M_{\rm pl}^2}{2}F(\phi)R + (1-6Q^2)F(\phi)X - V(\phi) + \beta_3 M^{-3}X\Box\phi\right] + \mathcal{S}_m, \tag{2.1}$$

where g is the determinant of metric tensor $g_{\mu\nu}$, $X = -\partial_\mu\phi\partial^\mu\phi/2$ is the kinetic energy of a scalar field ϕ, and $F(\phi)$ and $V(\phi)$ are functions of ϕ. The couplings Q and β_3 are dimensionless constants, while M is a constant having a dimension of mass related to today's Hubble constant H_0 as

$$M = (M_{\rm pl}H_0^2)^{1/3}, \tag{2.2}$$

which is of order 10^{-22} GeV. The mass scale (2.2), which translates to the frequency $f \sim 100$ Hz, corresponds to the typical strong coupling scale of theories containing derivative self-interactions such as $X\Box\phi$ [57,58].

We assume that the effective field theory of dark energy is valid up to the mass scale $M \sim 10^{-22}$ GeV. In other words, we resort to the action (2.1) for studying the physics on scales larger than $\sim 10^6$ m. This includes the dynamics of late-time cosmic acceleration ($\sim 10^{26}$ m) and the earth-moon local system of LLR experiments ($\sim 10^8$ m). Below the length scale 10^6 m, some ultraviolet effects may come into play to approach the general relativistic behavior. Indeed, the possibility of recovering the GW value $c_t = 1$ above the frequency $f \sim 100$ Hz was discussed in Ref. [94]. This critical frequency is of the same order as the GW frequency observed by LIGO/Virgo [14], so there may be more general Horndeski theories realizing c_t very close to 1 for the frequency $f \geq 100$ Hz even if the deviation of c_t from 1 is large on cosmological scales. In this paper we do not pursue such a possibility, but we focus on the theory given by the action (2.1) in which $c_t = 1$ for any scales of interest.

The nonminimal coupling $F(\phi)$ is chosen to be of the form

$$F(\phi) = e^{-2Q(\phi-\phi_0)/M_{\rm pl}}, \tag{2.3}$$

where ϕ_0 is today's value of ϕ and hence $F(\phi_0) = 1$. We assume that the matter sector, which is described by the action $\mathcal{S}_m$ with the density ρ_m, is minimally coupled to gravity. The scalar field mediates fifth forces with the matter sector through the direct gravitational interaction characterized by the coupling Q.

If $\beta_3 = 0$, then the theories given by the action (2.1) are equivalent to BD theories [25] with the scalar potential $V(\phi)$. Indeed, by setting $\chi = F(\phi)$, the Lagrangian in the action (2.1) reduces to $L = \chi R/2 - \omega_{\rm BD}\partial_\mu\chi\partial^\mu\chi/(2\chi) - V(\phi(\chi))$ in the unit $M_{\rm pl} = 1$, where $\omega_{\rm BD}$ is the BD parameter

related to Q according to $3+2\omega_{\rm BD}=1/(2Q^2)$ [38]. In the original massless BD theories with $V(\phi)=0$, the coupling strength is constrained to be $|Q|\le 2.4\times 10^{-3}$ from the Cassini experiment [43].

For the coupling $|Q|>2.4\times 10^{-3}$, we require the existence of scalar potential $V(\phi)$ or field derivative interaction $X\Box\phi$ to screen fifth forces in the solar system. In the former case, the chameleon mechanism [44,45] can be at work for the potential having a large mass in regions of high density. One of such examples is $f(R)$ gravity, in which the scalar potential of the gravitational origin arises with the coupling $Q=-1/\sqrt{6}$ [39]. In $f(R)$ models of late-time cosmic acceleration accommodating the chameleon mechanism in overdensity regions, the functional form of $f(R)$ needs to be designed such that the scalaron mass M_ϕ grows very rapidly toward the asymptotic past [47–50]. This causes the fine-tuning problem of initial conditions of perturbations associated with the oscillating mode induced by the heavy mass [48,50,51].

Instead of resorting to the chameleon mechanism with a very massive scalar in overdensity regions, we consider the Galileon self-interaction $X\Box\phi$ to suppress fifth forces under the Vainshtein mechanism [56]. The scalar potential $V(\phi)$ of a light scalar is also taken into account as a source for the cosmic acceleration. Defining the dimensionless quantity

$$\lambda\equiv\frac{M_{\rm pl}}{V}\frac{{\rm d}V}{{\rm d}\phi}, \tag{2.4}$$

the condition for cosmic acceleration in the absence of Galileon interactions and matter is given by $|\lambda|<\sqrt{2}$ [95,96]. The existence of Galileons can modify this structure, but we focus on the case in which the condition

$$|\lambda|\le\mathcal{O}(1) \tag{2.5}$$

is satisfied during the cosmic expansion history from the past to today. The coupling strength $|Q|$ exceeding the order 1 leads to the strong enhancement of matter density perturbations incompatible with observations in large-scale structures [38], so we consider the coupling

$$|Q|\le\mathcal{O}(0.1) \tag{2.6}$$

in the following discussion.

The original Galileon theory [21] has the linear potential $V(\phi)=m^3\phi$ with $Q=0$, in which case the resulting field equation of motion respects the Galilean symmetry in Minkowski spacetime. This potential corresponds to a massless scalar with $\lambda=M_{\rm pl}/\phi$, so the condition (2.5) translates to $\phi\ge M_{\rm pl}$. For $Q\neq 0$, the cosmological dynamics with the linear potential was studied in Ref. [78]. In this case, today's cosmic acceleration is followed by the collapsing universe after the field enters the region $V(\phi)<0$.

The constant λ corresponds to the exponential potential $V(\phi)=V_0e^{\lambda\phi/M_{\rm pl}}$. In this case, the scalar mass squared $M_\phi^2\equiv{\rm d}^2V/{\rm d}\phi^2$ is given by $M_\phi^2=\lambda^2V/M_{\rm pl}^2$. Since the potential energy V is the dominant contribution to today's energy density of the Universe, we have $V\lesssim M_{\rm pl}^2H^2$, where H is the Hubble expansion rate in the past (redshift $z\ge 0$). Then, under the condition (2.5), it follows that $M_\phi^2\lesssim\lambda^2H^2\lesssim H^2$. This property also holds for the potential with a time-varying λ in the range (2.5). For the light scalar whose mass M_ϕ today is smaller than H_0, the effect of M_ϕ on the scalar-field equation can be ignored to study the Vainshtein mechanism in regions of high density. In other words, the chameleon mechanism does not come into play for screening fifth forces.

A. Vainshtein screening

The behavior of scalar and gravitational fields around a spherically symmetric overdensity on a cosmological background was already studied in Refs. [62,64], so we briefly review it in the following. Let us consider the following perturbed metric in the Newtonian gauge:

$${\rm d}s^2=-(1+2\Psi){\rm d}t^2+(1+2\Phi)a^2(t)\delta_{ij}{\rm d}x^i{\rm d}x^j, \tag{2.7}$$

where $a(t)$ is the time-dependent scale factor, Ψ and Φ are gravitational potentials depending on t, and the radial coordinate $r=a(t)\sqrt{\delta_{ij}x^ix^j}$. The scalar field and matter density on the homogenous cosmological background are given by $\bar\phi(t)$ and $\bar\rho_m(t)$, respectively. The existence of a compact object gives rise to the perturbations $\chi(t,r)$ and $\delta\rho_m(t,r)$ in ϕ and ρ_m, such that $\phi=\bar\phi(t)+\chi(t,r)$ and $\rho_m=\bar\rho_m(t)+\delta\rho_m(t,r)$.

We are interested in solutions deep inside today's Hubble radius, $r\ll H_0^{-1}$. Hence we neglect time derivatives of perturbed quantities, while keeping spatial derivatives. The radial dependence of the derivative $\partial\chi/\partial r$ changes around the Vainshtein radius r_V, which is estimated as [63,64]

$$r_V\simeq\left(\frac{|\beta_3Q|M_{\rm pl}r_g}{M^3}\right)^{1/3}=(|\beta_3Q|r_gH_0^{-2})^{1/3}, \tag{2.8}$$

where

$$r_g=M_{\rm pl}^{-2}\int_0^r\delta\rho_m\tilde r^2{\rm d}\tilde r \tag{2.9}$$

is the Schwarzschild radius of the source. For $r\gg r_V$ the field derivative has the dependence $\partial\chi/\partial r\propto r^{-2}$, while, for $r\ll r_V$, $\partial\chi/\partial r\propto r^{-1/2}$. In the latter regime, the nonlinear effect arising from the cubic Galileon self-interaction suppresses the propagation of fifth forces induced by the coupling Q. Indeed, for $r\ll r_V$, the gravitational potentials are given by [63,64]

$$\Psi \simeq -\frac{r_g}{2rF}\left[1+\mathcal{O}(1)Q^2\left(\frac{r}{r_V}\right)^{3/2}\right], \tag{2.10}$$

$$\Phi \simeq \frac{r_g}{2rF}\left[1+\mathcal{O}(1)Q^2\left(\frac{r}{r_V}\right)^{3/2}\right]. \tag{2.11}$$

Since the value of F today (cosmic time t_0) is equivalent to 1 in our theory, the Newtonian behavior $[-\Psi=\Phi=r_g/(2r)]$ is recovered for $r \ll r_V$. As long as r_V is much larger than the solar-system scale ($\sim 10^{15}$ cm), the model is consistent with solar-system tests of gravity. Since $(r_g H_0^{-2})^{1/3} \simeq 3\times 10^{20}$ cm for the Sun, this condition translates to

$$|\beta_3 Q| \gg 10^{-17}. \tag{2.12}$$

When $|Q|$ is of order 10^{-2}, for example, the coupling β_3 needs to be in the range $|\beta_3| \gg 10^{-15}$.

B. LLR constraints

From Eqs. (2.10) and (2.11) with Eq. (2.9), the leading-order gravitational potentials deep inside the Vainshtein radius can be expressed as

$$-\Psi \simeq \Phi \simeq \frac{G_{\rm N}\delta\mathcal{M}}{r}, \tag{2.13}$$

where $\delta\mathcal{M}=4\pi\int_0^r \delta\rho_m \tilde{r}^2 {\rm d}\tilde{r}$, and $G_{\rm N}$ is the measured gravitational coupling given by

$$G_{\rm N}=\frac{1}{8\pi M_{\rm pl}^2 F(\phi(t))}, \tag{2.14}$$

where we omitted the bar from the background value of ϕ. Here the background field $\phi(t)$ is a cosmological scalar driving the late-time cosmic acceleration. Since we are considering overdensity regions on the cosmological background, the homogenous value $\phi(t)$ survives even in the local universe. The dark energy scalar field $\phi(t)$ changes in time, so this leads to the time variation of $G_{\rm N}$. This fact was first recognized in Ref. [62], and it was proved in Ref. [64] in full Horndeski theories.

The effective gravitational coupling (2.14) is valid for a light scalar field operated by the Vainshtein mechanism in overdensity regions. Here, the light scalar means that the slope of field potential $V(\phi)$ satisfies the condition (2.5). For the potential of a massive scalar violating this condition in regions of the high density [as in $f(R)$ dark energy models], the chameleon mechanism can be at work to suppress the gravitational coupling with matter in a way different from Eqs. (2.10) and (2.11). As we already mentioned, we do not consider such a massive scalar field in this paper.

For the cubic derivative self-interaction we chose the Galileon coupling $X\Box\phi$, but this can be generalized to the derivative coupling $X^n\Box\phi$ with $n>1$. In such cases, the second terms on the right-hand sides of (2.10) and (2.11) are modified to $\mathcal{O}(1)Q^2(r/r_V)^{2-1/(2n)}$, which is much smaller than 1 deep inside the Vainshtein radius. Then the local gravitational coupling reduces to the form (2.14), so the property of $G_{\rm N}$ induced by the time-dependent background scalar field $\phi(t)$ is similar to that of cubic Galileons. For the models in which derivative field self-interactions are not employed to screen fifth forces in overdensity regions, e.g., chameleons and nonlocal gravity, the expression of $G_{\rm N}$ is generally different from that discussed above.

From the recent LLR experiment, the variation of $G_{\rm N}$ is constrained to be [81]

$$\frac{\dot{G}_{\rm N}}{G_{\rm N}}=(7.1\pm 7.6)\times 10^{-14}\ {\rm yr}^{-1}, \tag{2.15}$$

where a dot represents the derivative with respect to t. This improves the previous bound $\dot{G}_{\rm N}/G_{\rm N}=(4\pm 9)\times 10^{-13}$ yr^{-1} [79]. Using the value $H_0=100h\,{\rm km\,s^{-1}\,Mpc^{-1}}=(9.77775\,{\rm Gyr})^{-1}h$, the bound (2.15) translates to [82]

$$\frac{\dot{G}_{\rm N}}{H_0 G_{\rm N}}=(0.99\pm 1.06)\times 10^{-3}\left(\frac{0.7}{h}\right). \tag{2.16}$$

We define the following quantity:

$$\alpha_{\rm M}\equiv\frac{\dot{F}}{HF}=-\frac{2Q\dot{\phi}}{M_{\rm pl}H}, \tag{2.17}$$

which was used in the context of effective field theory of dark energy [97]. Since $\alpha_{\rm M}$ is related to the variation of $G_{\rm N}$, as $\alpha_{\rm M}=-\dot{G}_{\rm N}/(HG_{\rm N})$, the bound (2.16) can be expressed as

$$-2.05\times 10^{-3}\left(\frac{0.7}{h}\right)\le\alpha_{\rm M}(t_0)\le 0.07\times 10^{-3}\left(\frac{0.7}{h}\right). \tag{2.18}$$

If $\alpha_{\rm M}>0$, i.e., for decreasing $G_{\rm N}$ in time, the upper bound is especially stringent: $\alpha_{\rm M}(t_0)\le 7\times 10^{-5}$ for $h=0.7$. Even when $\alpha_{\rm M}<0$, the upper limit of $|\alpha_{\rm M}(t_0)|$ is of the order 10^{-3}. They are smaller than the previous bound $|\alpha_{\rm M}(t_0)|\le 0.02$ [62] by more than 1 order of magnitude.

III. DYNAMICAL SYSTEM

We study the background cosmology for theories given by the action (2.1) and discuss how the coupling Q is constrained from the LLR bound (2.18). We consider the flat FLRW background described by the line element ${\rm d}s^2=-{\rm d}t^2+a^2(t)\delta_{ij}{\rm d}x^i{\rm d}x^j$. For the matter action $\mathcal{S}_m$, we take nonrelativistic matter (density ρ_m with vanishing pressure) and radiation (density ρ_r and pressure $P_r=\rho_r/3$)

into account. Then, the Hamiltonian and momentum constraints lead to [7,80]

$$3M_{\rm pl}^2H^2=\rho_{\rm DE}+\rho_m+\rho_r, \tag{3.1}$$

$$2M_{\rm pl}^2\dot{H}=-\rho_{\rm DE}-P_{\rm DE}-\rho_m-\frac{4}{3}\rho_r, \tag{3.2}$$

where $H=\dot{a}/a$ and $\rho_{\rm DE}$ and $P_{\rm DE}$ are the density and pressure of dark energy, defined, respectively, by

$$\rho_{\rm DE}=3M_{\rm pl}^2H^2(1-F)+\frac{F}{2}(1-6Q^2)\dot{\phi}^2 +6FQHM_{\rm pl}\dot{\phi}+V-3\beta_3M^{-3}H\dot{\phi}^3, \tag{3.3}$$

$$P_{\rm DE}=-M_{\rm pl}^2(2\dot{H}+3H^2)(1-F)+\frac{F}{2}(1+2Q^2)\dot{\phi}^2 -2FQM_{\rm pl}(\ddot{\phi}+2H\dot{\phi})-V+\beta_3M^{-3}\dot{\phi}^2\ddot{\phi}. \tag{3.4}$$

Besides the matter continuity equations $\dot{\rho}_m+3H\rho_m=0$ and $\dot{\rho}_r+4H\rho_r=0$, the dark sector obeys

$$\dot{\rho}_{\rm DE}+3H(\rho_{\rm DE}+P_{\rm DE})=0. \tag{3.5}$$

The dark energy equation of state is defined by

$$w_{\rm DE}\equiv\frac{P_{\rm DE}}{\rho_{\rm DE}}. \tag{3.6}$$

In nonminimally coupled theories the first terms on the right-hand sides of Eqs. (3.3) and (3.4) are different from 0 in the past due to the property $F\neq1$.

To study the background cosmological dynamics, we introduce the following density parameters:

$$\Omega_K\equiv\frac{\dot{\phi}^2}{6M_{\rm pl}^2H^2},\qquad \Omega_V\equiv\frac{V(\phi)}{3M_{\rm pl}^2H^2F},$$
$$\Omega_{G_3}\equiv-\frac{\beta_3\dot{\phi}^3}{M_{\rm pl}^2M^3HF},\qquad \Omega_r\equiv\frac{\rho_r}{3M_{\rm pl}^2H^2F}. \tag{3.7}$$

We consider the case in which Ω_{G_3} is positive in the expanding universe ($H>0$), which amounts to the condition

$$\beta_3\dot{\phi}<0. \tag{3.8}$$

We also define the quantity

$$x\equiv\frac{\dot{\phi}}{\sqrt{6}M_{\rm pl}H}, \tag{3.9}$$

which is related to Ω_K and $\alpha_{\rm M}$, as

$$\Omega_K=x^2,\qquad \alpha_{\rm M}=-2\sqrt{6}Qx. \tag{3.10}$$

We can express Eq. (3.1) in the form

$$\Omega_m\equiv\frac{\rho_m}{3M_{\rm pl}^2H^2F}=1-\Omega_{\rm DE}-\Omega_r, \tag{3.11}$$

where $\Omega_{\rm DE}$ is defined by

$$\Omega_{\rm DE}\equiv(1-6Q^2)\Omega_K-\alpha_{\rm M}+\Omega_V+\Omega_{G_3}. \tag{3.12}$$

From Eqs. (3.2) and (3.5), it follows that

$$h\equiv\frac{\dot{H}}{H^2}=-\frac{1}{\mathcal{D}}[\Omega_{G_3}(6+2\Omega_r-6\Omega_V+3\Omega_{G_3}-\alpha_{\rm M}+\sqrt{6}\Omega_V\lambda x)+2\Omega_K\{3+\Omega_r-3\Omega_V+6\Omega_{G_3}+6\lambda Q\Omega_V +6Q^2(1-\Omega_r+3\Omega_V-2\Omega_{G_3})\}-\alpha_{\rm M}\Omega_K(1-6Q^2)(2-\Omega_{G_3})+6\Omega_K^2(1-8Q^2+12Q^4)], \tag{3.13}$$

$$\epsilon_\phi\equiv\frac{\ddot{\phi}}{H\dot{\phi}}=\frac{1}{\mathcal{D}}[\Omega_{G_3}(\Omega_r-3-3\Omega_V)-\alpha_{\rm M}(\Omega_r-1-3\Omega_V-2\Omega_{G_3})-2\sqrt{6}\Omega_V\lambda x -3\Omega_K\{4(1-2Q^2)-\Omega_{G_3}(1+2Q^2)\}-\alpha_{\rm M}\Omega_K(5-6Q^2)], \tag{3.14}$$

where

$$\mathcal{D}=\Omega_{G_3}(4-2\alpha_{\rm M}+\Omega_{G_3})+4\Omega_K. \tag{3.15}$$

The condition for cosmic acceleration to occur is that the effective equation of state,

$$w_{\rm eff}\equiv-1-\frac{2}{3}h, \tag{3.16}$$

is smaller than $-1/3$.

The dimensionless variables x, Ω_V, Ω_{G_3}, and Ω_r obey the differential equations,

$$x'=x(\epsilon_\phi-h), \tag{3.17}$$

$$\Omega_V'=-\Omega_V(\alpha_{\rm M}-\sqrt{6}\lambda x+2h), \tag{3.18}$$

$$\Omega_{G_3}'=-\Omega_{G_3}(\alpha_{\rm M}-3\epsilon_\phi+h), \tag{3.19}$$

$$\Omega_r'=-\Omega_r(\alpha_{\rm M}+4+2h), \tag{3.20}$$

respectively, where a prime represents a derivative with respect to $\mathcal{N} = \ln a$. The dark energy equation of state (3.6) is expressed as

$$w_{\rm DE} = -\frac{3+2h-[3+2h+3(1+2Q^2)\Omega_K-3\Omega_V+\alpha_{\rm M}(2+\epsilon_\phi)-\epsilon_\phi\Omega_{G_3}]F}{3-3[1+(6Q^2-1)\Omega_K-\Omega_V+\alpha_{\rm M}-\Omega_{G_3}]F}. \tag{3.21}$$

The dimensionless field $y \equiv \phi/M_{\rm pl}$ obeys

$$y' = \sqrt{6}x. \tag{3.22}$$

Once the potential $V(\phi)$ is specified, the cosmological dynamics is known by solving Eqs. (3.17)–(3.20) and (3.22) for the given initial conditions of x, Ω_V, Ω_{G_3}, Ω_r, and y.

For the theory (2.1), the propagation speed squared of GWs is equivalent to 1 [7,98]. The tensor ghost is absent for $F(\phi) > 0$, which is satisfied for the choice (2.3). For scalar perturbations, the conditions for avoiding ghosts and Laplacian instabilities are given, respectively, by

$$q_s \equiv \Omega_{G_3}(4+\Omega_{G_3}-2\alpha_{\rm M})+4\Omega_K > 0, \tag{3.23}$$

$$c_s^2 \equiv \frac{\Omega_{G_3}[4(2+\epsilon_\phi)-\Omega_{G_3}-2\alpha_{\rm M}]+12\Omega_K}{3\Omega_{G_3}(4+\Omega_{G_3}-2\alpha_{\rm M})+12\Omega_K} > 0. \tag{3.24}$$

In Sec. IV, we will discuss whether these conditions are satisfied during the cosmological evolution from the radiation-dominated epoch to today.

IV. COSMOLOGICAL DYNAMICS

In this section, we study the cosmological dynamics for constant λ, i.e., the exponential potential,

$$V(\phi) = V_0 e^{\lambda\phi/M_{\rm pl}}. \tag{4.1}$$

In this case, the dynamical system given by Eqs. (3.17)–(3.20) is closed. As long as λ slowly varies in time in the range (2.5), the cosmological evolution is similar to that discussed below.

In overdensity regions of the Universe, the operation of the Vainshtein mechanism means that the cubic Galileon term $X\Box\phi$ dominates over other field Lagrangians. In the cosmological context, this amounts to the dominance of Ω_{G_3} over Ω_K and Ω_V in the early epoch. Let us consider the case in which the conditions

$$\{\Omega_K, \Omega_V\} \ll \Omega_{G_3} \ll 1, \qquad |\alpha_{\rm M}| \ll 1, \tag{4.2}$$

are satisfied during the radiation-dominated epoch (in which Ω_r is close to 1). From Eqs. (3.13) and (3.14), we then have $h \simeq -2$ and

$$\epsilon_\phi \simeq -\frac{1}{2}+\epsilon_\alpha, \qquad \epsilon_\alpha \equiv \frac{\alpha_{\rm M}}{4\Omega_{G_3}}(1-\Omega_r). \tag{4.3}$$

Since Ω_r starts to deviate from 1 in the late radiation era, the term ϵ_α is not necessarily negligible relative to $-1/2$ for $|\alpha_{\rm M}| \gg \Omega_{G_3}$. On using Eqs. (3.17), (3.19), and (3.20), the quantity ϵ_α obeys the differential equation,

$$\epsilon_\alpha' \simeq 6Q^2\frac{\Omega_K}{\Omega_{G_3}}+2\epsilon_\alpha(1-\epsilon_\alpha). \tag{4.4}$$

Under the condition $\Omega_{G_3} \gg \Omega_K$, the first term on the right-hand side of Eq. (4.4) is much smaller than 1. Ignoring this term and solving the differential equation $\epsilon_\alpha' \simeq 2\epsilon_\alpha(1-\epsilon_\alpha)$ for ϵ_α, it follows that

$$\epsilon_\alpha = \left[1+\frac{a_i^2}{a^2}\frac{1-\epsilon_\alpha^{(i)}}{\epsilon_\alpha^{(i)}}\right]^{-1}, \tag{4.5}$$

where $\epsilon_\alpha^{(i)}$ is the initial value of ϵ_α at $a = a_i$. In the limit $a \to \infty$, ϵ_α asymptotically approaches 1.

If the condition $|\alpha_{\rm M}| \gg \Omega_{G_3}$ is initially satisfied, $|\epsilon_\alpha^{(i)}|$ can be as large as the order 1. Then, ϵ_ϕ soon approaches the asymptotic value

$$\epsilon_\phi \to \frac{1}{2}, \tag{4.6}$$

during the radiation era. In this regime, the field density parameters and $|\alpha_{\rm M}|$ grow as

$$\Omega_K \propto a^5, \qquad \Omega_V \propto a^4, \qquad \Omega_{G_3} \propto a^{7/2}, \qquad |\alpha_{\rm M}| \propto a^{5/2}. \tag{4.7}$$

This shows that, even if $\Omega_{G_3} \gg \Omega_K$ initially, it is possible for Ω_K to catch up with Ω_{G_3}. If this catch-up occurs by the end of the radiation era, we have $\Omega_{G_3} < \Omega_K$ at the onset of matter dominance.

If $|\alpha_{\rm M}| \ll \Omega_{G_3}$ initially, i.e., $|\epsilon_\alpha^{(i)}| \ll 1$, there is the stage of radiation era in which the quantity ϵ_ϕ is close to $-1/2$. On using Eqs. (3.17)–(3.19) in this epoch, the field density parameters and $|\alpha_{\rm M}|$ evolve as

$$\Omega_K \propto a^3, \qquad \Omega_V \propto a^4, \qquad \Omega_{G_3} \propto a^{1/2}, \qquad |\alpha_{\rm M}| \propto a^{3/2}, \tag{4.8}$$

so that $|\alpha_{\rm M}|$ grows faster than Ω_{G_3}. If $|\alpha_{\rm M}|$ exceeds Ω_{G_3} during the radiation era, the solutions enter the regime characterized by Eqs. (4.6) and (4.7). Although Ω_K grows faster than Ω_{G_3} in the two regimes explained above, it can happen that the inequality $\Omega_{G_3} > \Omega_K$ still holds at the beginning of the matter era for Ω_{G_3} initially much larger than $|\alpha_{\rm M}|$ and Ω_K.

The above discussion shows that there are two qualitatively different cases depending on the values of Ω_{G_3} and Ω_K at the onset of matter dominance. The first is the case in which Ω_K dominates over Ω_{G_3}, i.e.,

$$\text{(i)} \quad \Omega_{G_3} \ll \Omega_K \quad \text{(unscreened)}. \tag{4.9}$$

Under this condition, there exists the ϕMDE in which the field kinetic energy is not screened by the Galileon term.

The second is the case in which the condition

$$\text{(ii)} \quad \Omega_{G_3} \gg \Omega_K \quad \text{(screened)} \tag{4.10}$$

is satisfied after the end of the radiation era. This corresponds to the situation in which the cosmological Vainshtein screening is sufficiently efficient to suppress the time variation of ϕ throughout the evolution from the radiation era to today. In the following, we study these two different cases in turn.

We note that, under the conditions (4.2), the dark energy equation of state (3.21) during the radiation dominance can be estimated as

$$w_{\rm DE} \simeq w_{\rm eff} \simeq \frac{1}{3}, \tag{4.11}$$

irrespective of the two asymptotic values of $\epsilon_\phi (= \pm 1/2)$ explained above.

A. Unscreened late-time cosmology with the ϕMDE

Let us first study the cosmological dynamics for the case (i), i.e., $\Omega_{G_3} \ll \Omega_K$ after the onset of the matter era. In this case, the coupling β_3 is in the range

$$|\beta_3| \ll 1. \tag{4.12}$$

To derive fixed points of the dynamical system, we take the limit $\Omega_{G_3} \to 0$ in the autonomous Eqs. (3.17)–(3.20). For $Q \neq 0$, the standard matter era is replaced by the ϕMDE characterized by the fixed point

$$\text{(a)} \quad (x, \Omega_V, \Omega_{G_3}, \Omega_r) = \left(-\frac{\sqrt{6}Q}{3(1-2Q^2)}, 0, 0, 0 \right), \tag{4.13}$$

with

$$\Omega_m = \frac{3-2Q^2}{3(1-2Q^2)^2}, \qquad w_{\rm eff} = \frac{4Q^2}{3(1-2Q^2)},$$
$$w_{\rm DE} = \frac{4Q^2(1-2Q^2)}{3(1-F)-2(6-F)Q^2+12Q^4}. \tag{4.14}$$

The ϕMDE was originally found for coupled quintessence in the Einstein frame [83]. This corresponds to the kinetically driven stage in which $\Omega_K = 2Q^2/[3(1-2Q^2)^2]$ dominates over Ω_{G_3}. On the fixed point (a), the parameter $\alpha_{\rm M}$ is given by

$$\alpha_{\rm M}^{(\rm a)} = \frac{4Q^2}{1-2Q^2}, \tag{4.15}$$

and hence $\alpha_{\rm M}^{(\rm a)} > 0$ for $Q^2 < 1/2$. The positivity of $\alpha_{\rm M}^{(\rm a)}$ means that

$$Q x_{(\rm a)} < 0, \tag{4.16}$$

where $x_{(\rm a)}$ is the value of x on the ϕMDE.

After Ω_K exceeds Ω_{G_3} by the end of the radiation era, the solutions are naturally followed by the ϕMDE in which the cosmological Vainshtein screening is no longer effective. While Ω_K is constant during the ϕMDE, the other field density parameters evolve as

$$\Omega_V \propto a^{\frac{3-2Q\lambda-6Q^2}{1-2Q^2}}, \qquad \Omega_{G_3} \propto a^{\frac{3+2Q^2}{1-2Q^2}}. \tag{4.17}$$

For $|Q\lambda| \ll 1$ and $Q^2 \ll 1$, Ω_V grows in proportion to a^3, whereas Ω_{G_3} decreases as $\propto a^{-3}$. Hence the contribution of cubic Galileons to $\Omega_{\rm DE}$ becomes negligibly small in the late matter era.

The stability of point (a) is known by linearly perturbing Eqs. (3.17)–(3.20) with homogenous perturbations δx, $\delta\Omega_V$, $\delta\Omega_{G_3}$, and $\delta\Omega_r$ [95,96]. The eigenvalues of the Jacobian matrix associated with these perturbations are given by -1, $-(3-2Q^2)/(2-4Q^2)$, $-(3+2Q^2)/(1-2Q^2)$, and $(3-2Q\lambda-6Q^2)/(1-2Q^2)$. The first three eigenvalues are negative for λ and Q in the ranges (2.5) and (2.6), while the last one is positive. Hence the ϕMDE corresponds to a saddle point. This shows that, as long as Ω_K catches up with Ω_{G_3} by the end of the radiation era, the solutions temporally approach the ϕMDE with $\Omega_{G_3} \ll \Omega_K \simeq$ const.

There are other kinetically driven fixed points characterized by $(x, \Omega_V, \Omega_{G_3}, \Omega_r) = (1/(\sqrt{6}Q \pm 1), 0, 0, 0)$. Since $\Omega_m = 0$, this point cannot be responsible for the matter era. The scaling fixed point $(x, \Omega_V, \Omega_{G_3}, \Omega_r) = (-\sqrt{6}/(2\lambda), (3-2Q\lambda-6Q^2)/(2\lambda^2), 0, 0)$ is also present, but $\Omega_{\rm DE} = (3 - 7Q\lambda - 12Q^2)/\lambda^2$ is larger than the order 1 under the conditions (2.5) and (2.6). Hence this scaling solution is irrelevant to the matter-dominated epoch. This is also the case for the radiation scaling solution $(x, \Omega_V, \Omega_{G_3}, \Omega_r) = (-2\sqrt{6}/(3\lambda), 4/(3\lambda^2), 0, 1 - 4(1 - 2Q\lambda - 4Q^2)/\lambda^2)$, where $\Omega_{\rm DE} = 4(1 - 2Q\lambda - 4Q^2)/\lambda^2$ exceeds the order 1.

The fixed point relevant to the dark energy domination is given by

$$\text{(b)} \quad (x, \Omega_V, \Omega_{G_3}, \Omega_r) = \left(\frac{-\sqrt{6}(\lambda+4Q)}{6(1-Q\lambda-4Q^2)}, \frac{6-\lambda^2-8Q(\lambda+2Q)}{6(1-Q\lambda-4Q^2)^2}, 0, 0 \right), \tag{4.18}$$

with

$$\Omega_m = 0, \qquad w_{\rm eff} = w_{\rm DE} = -1 + \frac{\lambda^2+6Q\lambda+8Q^2}{3(1-Q\lambda-4Q^2)}, \tag{4.19}$$

and $\Omega_{\rm DE} = 1$. On this fixed point, the quantity $\alpha_{\rm M}$ yields

$$\alpha_{\rm M}^{(\rm b)} = \frac{2Q(\lambda+4Q)}{1-Q\lambda-4Q^2}. \tag{4.20}$$

The point (b) can drive the cosmic acceleration for $w_{\rm eff} < -1/3$, which translates to

$$\lambda^2 < 2(1-4Q\lambda-8Q^2). \tag{4.21}$$

Under this bound, the four eigenvalues of the Jacobian matrix of homogenous perturbations around point (b) are all negative. Then, after the ϕMDE, the solutions finally approach the stable point (b) with cosmic acceleration. On using the values of x and Ω_V in Eq. (4.18), Eq. (3.19) reduces to

$$\Omega'_{G_3} = -p\Omega_{G_3}, \qquad p = \frac{(\lambda+4Q)^2}{1-Q\lambda-4Q^2}. \tag{4.22}$$

The Galileon density parameter decreases as $\Omega_{G_3} \propto a^{-p}$ around point (b).

In the following, we focus on the couplings satisfying

$$\lambda > 0, \qquad Q > 0. \tag{4.23}$$

During the ϕMDE, we showed that $\alpha_{\rm M} > 0$ for $Q^2 < 1/2$. Provided x does not change the sign during the cosmological evolution from the radiation era to fixed point (b), the parameter $\alpha_{\rm M}$ is in the range

$$\alpha_{\rm M} = -2\sqrt{6}Qx > 0, \tag{4.24}$$

and hence $x < 0$. The negative value of x is consistent with the fact that $\dot\phi < 0$ when the scalar field rolls down the potential with $\lambda > 0$. Alternatively, we can consider negative values of λ and Q, in which case $x > 0$. Under the condition (4.24), we have $Q\dot\phi < 0$ for $H > 0$ and hence the quantity $Q\phi$ decreases in time. This means that the field ϕ satisfies the inequality $Q(\phi-\phi_0) > 0$ in the past. Then, irrespective of the sign of Q, the quantity $F = e^{-2Q(\phi-\phi_0)/M_{\rm pl}}$ is smaller than 1 during the past cosmic expansion history.

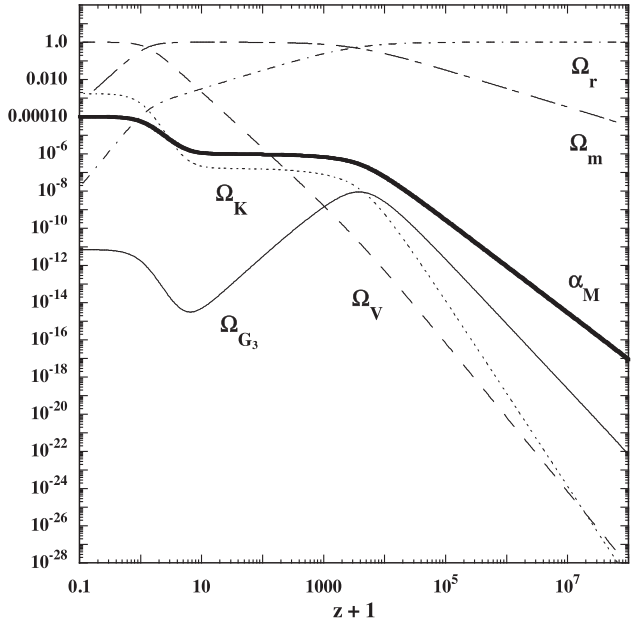

FIG. 1. Evolution of $\Omega_K, \Omega_V, \Omega_{G_3}, \Omega_m, \Omega_r$, and $\alpha_{\rm M}$ versus $z+1$ for $Q = 5.0\times10^{-4}$ and $\lambda = 0.1$ with the initial conditions $x = -1.0\times10^{-15}$, $\Omega_V = 1.0\times10^{-29}$, $\Omega_{G_3} = 1.0\times10^{-23}$, $\Omega_r = 0.99998$, and $y = 1.0$ at the redshift $z = 1.62\times10^8$. The present epoch ($z = 0$) is identified by the condition $\Omega_{\rm DE} = 0.68$.

In Fig. 1, we exemplify the evolution of Ω_K, Ω_V, Ω_{G_3}, Ω_r, Ω_m, and $\alpha_{\rm M}$ versus $z+1 (= a(t_0)/a(t))$ for $Q = 5.0\times10^{-4}$ and $\lambda = 0.1$. In this case, the initial value of ϵ_α in Eq. (4.3) is $\epsilon_\alpha^{(i)} = 1.22$, so ϵ_ϕ starts from the value around 0.72. As estimated from Eq. (4.6), ϵ_ϕ soon approaches the value $1/2$ during the radiation era. In Fig. 1, we can confirm that the evolution of Ω_K, Ω_V, Ω_{G_3}, and $\alpha_{\rm M}$ around the redshift $10^4 \lesssim z \lesssim 10^8$ is approximately given by Eq. (4.7). In Fig. 2, we plot the evolution of $w_{\rm DE}$ and $w_{\rm eff}$ for the same model parameters and initial conditions as those used in Fig. 1. As the analytic estimation (4.11) shows, both $w_{\rm DE}$ and $w_{\rm eff}$ are close to $1/3$ during the deep radiation-dominated epoch.

In the numerical simulation of Fig. 1, Ω_K catches up with Ω_{G_3} around the redshift $z = 4.6\times10^3$. Then, the solutions approach the ϕMDE with the constant kinetic density parameter $\Omega_K = 2Q^2/[3(1-2Q^2)^2] \simeq 1.7\times10^{-7}$ with $\alpha_{\rm M} = 6(1-2Q^2)\Omega_K \simeq 1.0\times10^{-6}$. As we estimated in Eq. (4.17), Ω_V increases during the ϕMDE, while Ω_{G_3} decreases. In Fig. 1, we observe that Ω_V exceeds $\alpha_{\rm M}$ around the redshift $z = 130$. After this moment, Ω_V becomes the dominant contribution to $\Omega_{\rm DE}$. As long as $\Omega_V \ll 1$, the terms containing Ω_V in Eqs. (3.13) and (3.14) hardly modify the values of h and ϵ_ϕ during the ϕMDE. In Fig. 1, we find that the ϕMDE with nearly constant Ω_K continues up to the redshift $z \approx 10$.

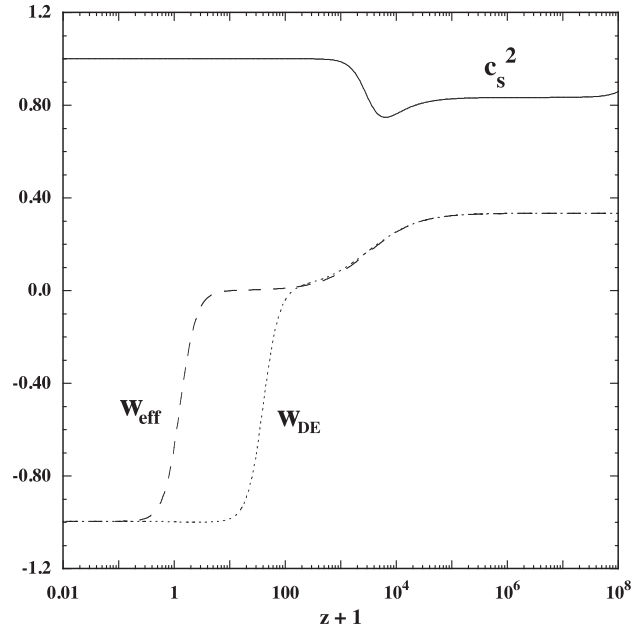

FIG. 2. Evolution of $w_{\rm DE}$, $w_{\rm eff}$, and c_s^2 versus $z+1$ for the same model parameters and initial conditions as those given in the caption of Fig. 1.

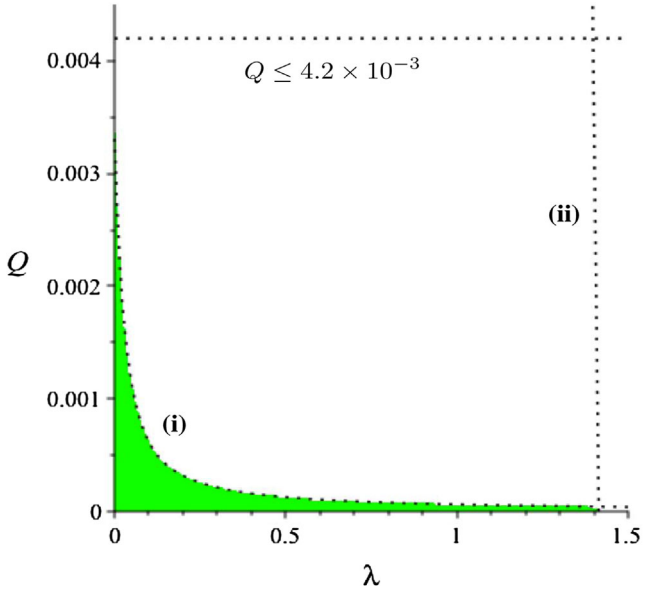

FIG. 3. Parameter space in the (λ, Q) plane (colored region) consistent with the bound (i) $\alpha_{\rm M}(t_0) \le 7 \times 10^{-5}$, and (ii) the condition for the cosmic acceleration of point (b). We also show the bound $Q \le 4.2 \times 10^{-3}$ arising from the condition $\alpha_{\rm M}^{(a)} \le 7 \times 10^{-5}$ on the ϕMDE.

The dark energy equation of state is more sensitive to the dominance of Ω_V over other field density parameters. In the regime where the condition $\Omega_V \gg \{\alpha_{\rm M}, \Omega_K, \Omega_{G_3}\}$ is satisfied, Eq. (3.21) approximately reduces to

$$w_{\rm DE} \simeq -1 - \frac{2h}{3}\frac{1-F}{1-F+\Omega_V F}. \tag{4.25}$$

Provided the inequality $\Omega_V F \ll 1-F$ holds during the early stage of the matter era, it follows that $w_{\rm DE} \simeq w_{\rm eff} = -1 - 2h/3 \simeq 4Q^2/[3(1-2Q^2)]$. After $\Omega_V F$ grows to be larger than $1-F$, $w_{\rm DE}$ starts to approach -1. In Fig. 2, we can confirm that $w_{\rm DE}$ deviates from $w_{\rm eff}$ around the same moment at which Ω_V becomes the dominant contribution to $\Omega_{\rm DE}$ and that $w_{\rm DE}$ temporally approaches the value close to -1.

After the Universe enters the stage of cosmic acceleration, the solutions finally reach the fixed point (b). For $Q = 5.0 \times 10^{-4}$ and $\lambda = 0.1$, the analytic estimation (4.18) gives the values $x = -0.04164$, $\Omega_V = 0.9984$, and $w_{\rm DE} = w_{\rm eff} = -0.9966$, which are in good agreement with the numerical results of Figs. 1 and 2. In this case, the future asymptotic value of $\alpha_{\rm M}$ is 1.02×10^{-4}, while its value today is $\alpha_{\rm M}(t_0) = 5.61 \times 10^{-5}$. Taking $h = 0.7$ in Eq. (2.18), this case is within the LLR bound of $\alpha_{\rm M}(t_0)$.

From Eqs. (4.13) and (4.18) we find that the inequality $0 > x_{\rm (a)} > x_{\rm (b)}$ holds, where $x_{\rm (a)}$ and $x_{\rm (b)}$ are the values of x on points (a) and (b), respectively. Then, the quantity $\alpha_{\rm M}$ on point (b) is larger than that on point (a), such that $\alpha_{\rm M}^{(b)} > \alpha_{\rm M}^{(a)} > 0$. Since $\alpha_{\rm M}$ increases from $\alpha_{\rm M}^{(a)}$ during the ϕMDE to the asymptotic value $\alpha_{\rm M}^{(b)}$ in the future, the necessary condition for satisfying the LLR bound (2.18) for $h = 0.7$ is $\alpha_{\rm M}^{(a)} \le 7 \times 10^{-5}$, i.e.,

$$Q \le 4.2 \times 10^{-3}. \tag{4.26}$$

Since today's value $\alpha_{\rm M}(t_0)$ is between $\alpha_{\rm M}^{(b)}$ and $\alpha_{\rm M}^{(a)}$, the condition (4.26) is not sufficient for the compatibility with the bound (2.18).

In Fig. 3, we plot the parameter space in the (λ, Q) plane constrained from the bound $\alpha_{\rm M}(t_0) \le 7 \times 10^{-5}$, whose border is denoted as the line (i). We also depict the region in which the condition (4.21) for cosmic acceleration of point (b) is satisfied, whose border is shown as the line (ii). This condition gives the upper limit $\lambda < \sqrt{2}$. The coupling Q is constrained to be

$$Q \le 3.4 \times 10^{-3}, \tag{4.27}$$

which is tighter than (4.26). This significantly improves the upper limit $Q \le 2.6 \times 10^{-2}$ following from the LLR bound $|\alpha_{\rm M}(t_0)| \le 0.02$ in 2004 [62]. We note that the bound (4.27) corresponds to the limit $\lambda \to 0$. For increasing λ from 0, the constraint on Q is more stringent than (4.27), e.g., $Q \le 6.2 \times 10^{-4}$ for $\lambda = 0.1$ and $Q \le 6.3 \times 10^{-5}$ for $\lambda = 1$. If $\lambda > 0.013$, then the recent LLR data give the upper limit of Q tighter than the Cassini bound $Q \le 2.4 \times 10^{-3}$ derived for the massless scalar field without the Vainshtein screening.

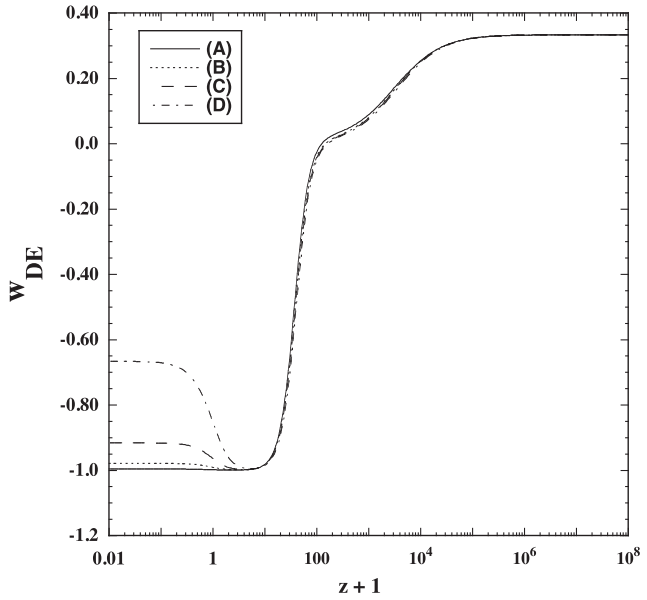

FIG. 4. Evolution of $w_{\rm DE}$ versus $z+1$ for (A) $Q = 6.20 \times 10^{-4}$, $\lambda = 0.1$; (B) $Q = 2.57 \times 10^{-4}$, $\lambda = 0.25$; (C) $Q = 1.27 \times 10^{-4}$, $\lambda = 0.5$; and (D) $Q = 6.32 \times 10^{-5}$, $\lambda = 1$. The initial conditions of x, Ω_V, Ω_{G_3}, Ω_r, and y are the same as those used in Fig. 1.

Cosmologically, today's value of Ω_{G_3} is related to the dimensionless coupling β_3, as

$$\Omega_{G_3}(t_0) = -6\sqrt{6}\beta_3 x(t_0)^3. \tag{4.28}$$

The numerical simulation of Fig. 1 corresponds to $\Omega_{G_3}(t_0) = 1.76 \times 10^{-12}$, $x(t_0) = -2.29 \times 10^{-2}$, and $\beta_3 = 9.97 \times 10^{-9}$, with $Q = 5.0 \times 10^{-4}$. These couplings satisfy the condition (2.12), so the Vainshtein mechanism is at work in the solar system. The existence of ϕMDE generally requires that $\beta_3 \ll 1$, but still the fifth force can be screened around local sources for the product $\beta_3 Q$ in the range (2.12).

In Fig. 4, we show the evolution of $w_{\rm DE}$ for four different combinations of Q and λ. In all these cases, $\alpha_{\rm M}(t_0)$ is close to the LLR upper limit 7×10^{-5}, with β_3 of order 10^{-8}. As we estimated in Eq. (4.25), $w_{\rm DE}$ temporally approaches the value close to -1 after Ω_V dominates over other field density parameters in the matter era. In all the cases plotted in Fig. 4, the minimum values of $w_{\rm DE}$ are close to -1. Even for case (D), i.e., $\lambda = 1$, $w_{\rm DE}$ reaches the minimum value -0.9952 at $z = 4.5$. The solutions finally approach the fixed point (b), with $w_{\rm DE}$ given by Eq. (4.19). For larger λ closer to the border line (ii) in Fig. 3, the deviation of $w_{\rm DE}$ from -1 at low redshifts is more significant. This property can be used to distinguish between the models with different values of λ from observations.

Since Ω_{G_3} and Ω_K are positive with $0 < \alpha_{\rm M} \ll 1$ from the radiation era to the accelerated point (b), the no-ghost condition (3.23) of scalar perturbations is always satisfied. Provided that $1 \gg \Omega_{G_3} \gg \Omega_K$ in the deep radiation era, the scalar propagation speed squared (3.24) reduces to $c_s^2 \simeq (2+\epsilon_\phi)/3$. In the numerical simulation of Fig. 2, the quantity ϵ_ϕ approaches the value $1/2$ around the redshift $z \approx 10^7$, and hence $c_s^2 \simeq 5/6$ for $10^5 \lesssim z \lesssim 10^7$. During the late radiation era ($3000 \lesssim z \lesssim 10^5$) in which Ω_r starts to deviate from 1, c_s^2 temporally decreases due to the decrease of ϵ_ϕ. For $\Omega_K \gg \Omega_{G_3}$ we have $c_s^2 \simeq 1$ from Eq. (3.24). Indeed, the approach to this value can be confirmed in Fig. 2 after the onset of the matter era. Since c_s^2 remains positive from the radiation era to the asymptotic future, the Laplacian instability of scalar perturbations is absent. We note that the property $c_s^2 > 0$ also holds for the four cases shown in Fig. 4.

B. Screened cosmology

We proceed to the case (ii) in which the cubic coupling β_3 is in the range

$$|\beta_3| \gg 1, \tag{4.29}$$

with positive values of λ and Q. As we will see below, the field kinetic energy can be suppressed even in the late epoch through the cosmological Vainshtein mechanism.

During the radiation dominance the condition (4.2) holds, so the quantity ϵ_ϕ can be estimated as Eq. (4.3). The difference from the case discussed in Sec. IV A is that ϵ_α is much smaller than 1 due to the largeness of Ω_{G_3} relative to $\alpha_{\rm M}$. Since $\epsilon_\phi \simeq -1/2$ during most stages of the radiation era, the field density parameters and $\alpha_{\rm M}$ evolve according to Eq. (4.8). Indeed, we can confirm this behavior in Fig. 5, where the cubic coupling is $\beta_3 = 1.0 \times 10^7$. Although Ω_K grows faster than Ω_{G_3}, the inequality $\Omega_{G_3} \gg \Omega_K$ holds even after the end of the radiation era. Hence the solutions do not reach the ϕMDE charactrized by constant Ω_K larger than Ω_{G_3}. In Fig. 6, we observe that both $w_{\rm DE}$ and $w_{\rm eff}$ are close to $1/3$ during the radiation dominance.

During the matter-dominated epoch, we study the cosmological evolution under the conditions

$$\Omega_K \ll \Omega_{G_3} \ll 1, \qquad \alpha_{\rm M} \ll 1, \qquad \Omega_V \ll 1,$$
$$\Omega_r \ll 1, \qquad (\lambda/Q)\Omega_V \ll 1. \tag{4.30}$$

Then, the quantities defined in Eqs. (3.13) and (3.14) reduce to $h \simeq -3/2$ and $\epsilon_\phi \simeq -3/4 + \alpha_{\rm M}/(4\Omega_{G_3})$, respectively. From Eqs. (3.17)–(3.19), we obtain the differential equations for $\alpha_{\rm M}$, Ω_V, and Ω_{G_3}, as

$$\alpha_{\rm M}' \simeq \frac{\alpha_{\rm M}}{4}\left(3 + \frac{\alpha_{\rm M}}{\Omega_{G_3}}\right), \tag{4.31}$$

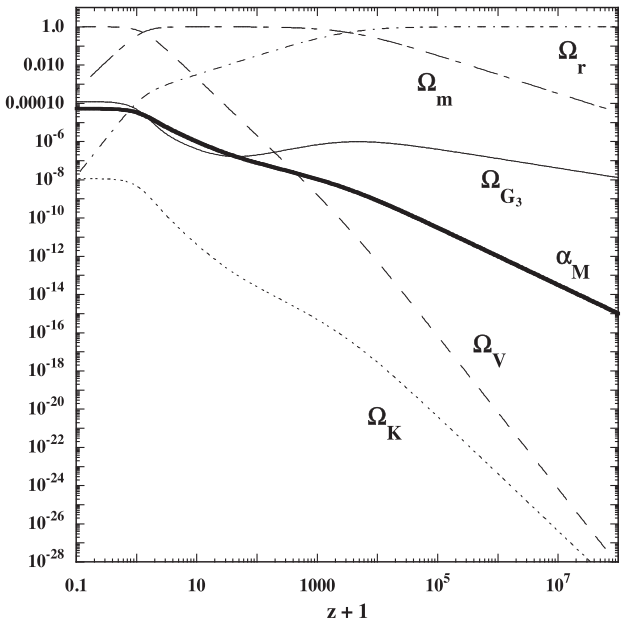

FIG. 5. Evolution of Ω_K, Ω_V, Ω_{G_3}, Ω_m, Ω_r, and $\alpha_{\rm M}$ versus $z+1$ for $Q=0.1$ and $\lambda=1$ with the initial conditions $x=-1.0\times10^{-15}$, $\Omega_V=1.0\times10^{-29}$, $\Omega_{G_3}=1.0\times10^{-8}$, $\Omega_r=0.99998$, and $y=1.0$ at the redshift $z=1.62\times10^8$.

$$\Omega_V' \simeq 3\Omega_V, \tag{4.32}$$

$$\Omega_{G_3}' \simeq -\frac{3}{4}(\Omega_{G_3}-\alpha_{\rm M}). \tag{4.33}$$

This means that, provided $x<0$, $\alpha_{\rm M}$ increases during the matter era. The density parameter associated with the field potential also grows as $\Omega_V \propto a^3$. On the other hand, Ω_{G_3} decreases for $\Omega_{G_3}>\alpha_{\rm M}$, whereas it increases for $\Omega_{G_3}<\alpha_{\rm M}$. In the numerical simulation of Fig. 5, Ω_{G_3} is larger than $\alpha_{\rm M}$ at the onset of the matter era and hence Ω_{G_3} decreases by the moment at which $\alpha_{\rm M}$ catches up with Ω_{G_3}. After this catch-up, Ω_{G_3} starts to grow. The field kinetic density parameter increases as $\Omega_K \propto \alpha_{\rm M}^2$, but still Ω_K is smaller than Ω_{G_3} around the end of matter era.

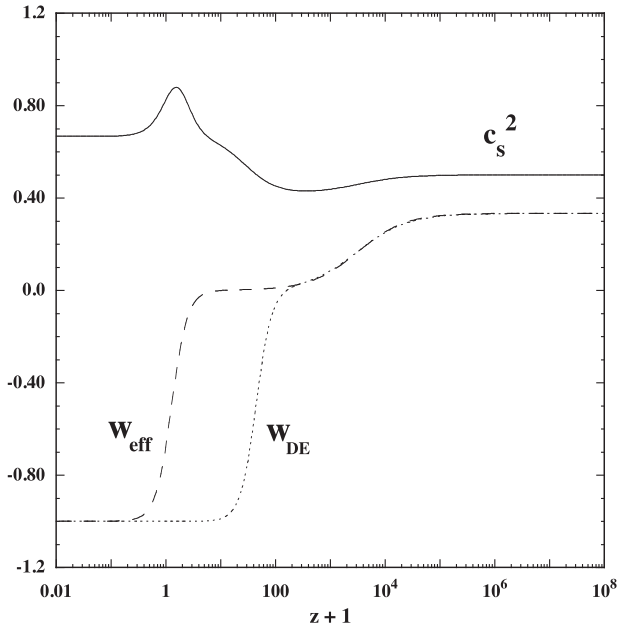

FIG. 6. Evolution of $w_{\rm DE}$, $w_{\rm eff}$, and c_s^2 versus $z+1$ for the same model parameters and initial conditions as those used in Fig. 5.

In Fig. 5, we find that Ω_V dominates over Ω_{G_3}, Ω_K, and $\alpha_{\rm M}$ for the redshift $z \lesssim 200$. Then, the dark energy equation of state after the dominance of Ω_V is given by Eq. (4.25). The numerical simulation of Fig. 6 shows that $w_{\rm DE}$ starts to deviate from $w_{\rm eff}\simeq 0$ around $z=200$ and then $w_{\rm DE}$ approaches the value close to -1 for $z \lesssim 10$. From the radiation dominance to the deep matter era, we have $\epsilon_\phi \simeq [\Omega_r - 3 + (1-\Omega_r)(\alpha_{\rm M}/\Omega_{G_3})]/4$ under the condition (4.30). Then, the sound speed squared $c_s^2 \simeq (2+\epsilon_\phi)/3$ can be estimated as

$$c_s^2 \simeq \frac{1}{12}\left[5+\Omega_r+\frac{\alpha_{\rm M}}{\Omega_{G_3}}(1-\Omega_r)\right], \tag{4.34}$$

which is valid for $z \gg 10$. As Ω_r starts to deviate from 1 in the late radiation era, c_s^2 decreases from the initial value close to $1/2$. Since the ratio $\alpha_{\rm M}/\Omega_{G_3}$ grows in the deep matter era, the term $(\alpha_{\rm M}/\Omega_{G_3})(1-\Omega_r)$ in Eq. (4.34) starts to increase the value of c_s^2. Indeed, in the numerical simulation of Fig. 6, c_s^2 reaches the minimum value 0.430 around $z=365$.

In Fig. 5, we observe that Ω_V, Ω_{G_3}, and Ω_K asymptotically approach constants with $\Omega_V=\mathcal{O}(1) \gg \Omega_{G_3} \gg \Omega_K$. In the regime where Ω_V dominates over Ω_{G_3}, Ω_K, and Ω_r, Eq. (3.17) approximately reduces to

$$x' \simeq \frac{x}{4}\left[3(1-3\Omega_V)-\frac{2\sqrt{6}x}{\Omega_{G_3}}\{Q+(3Q+\lambda)\Omega_V\}\right]. \tag{4.35}$$

Then, the solutions approaching a nonvanishing constant x are given by

$$x \simeq -\frac{\sqrt{6}(3\Omega_V-1)}{4[Q+(3Q+\lambda)\Omega_V]}\Omega_{G_3}. \tag{4.36}$$

Substituting this relation into Eqs. (3.18) and (3.19), it follows that

$$\Omega_V' \simeq 3\Omega_V(1-\Omega_V), \tag{4.37}$$

$$\Omega_{G_3}' \simeq 3(\Omega_V-1)\Omega_{G_3}, \tag{4.38}$$

which can be integrated to give

$$\Omega_V \simeq (1+c_1 a^{-3})^{-1}, \tag{4.39}$$

$$\Omega_{G_3} \simeq c_2(1 + c_1 a^{-3}), \tag{4.40}$$

where c_1 and c_2 are constants. These solutions are valid only at the very late cosmological epoch in which x starts to approach a constant. From Eqs. (4.39) and (4.40), Ω_V and Ω_{G_3} approach the values 1 and c_2, respectively. Taking the limit $\Omega_V \to 1$ in Eq. (4.36), we can estimate the asymptotic values of $\alpha_{\rm M}$ and the ratio Ω_K/Ω_{G_3}, as

$$\alpha_{\rm M} = \frac{6Q}{4Q+\lambda}\Omega_{G_3}, \tag{4.41}$$

$$\frac{\Omega_K}{\Omega_{G_3}} = \frac{3}{2(4Q+\lambda)^2}\Omega_{G_3}. \tag{4.42}$$

They are in good agreement with the numerical values in Fig. 5, i.e., $\alpha_{\rm M} = 5.24 \times 10^{-5}$ and $\Omega_K/\Omega_{G_3} = 9.37 \times 10^{-5}$ with $\Omega_{G_3} = 1.22 \times 10^{-4}$, so the condition $\Omega_{G_3} \gg \Omega_K$ is satisfied. We note that, for the other solution $x = 0$ in Eq. (4.35), Ω_{G_3} approaches 0, so this does not lead to the solution with $\Omega_{G_3} \gg \Omega_K > 0$.

In the numerical simulation of Fig. 5, today's value of $\alpha_{\rm M}$ is 3.38×10^{-5}, and hence this case is within the LLR bound (2.18). On using Eq. (4.41), the criterion for consistency with the LLR experiment is that the asymptotic value of Ω_{G_3} is in the range

$$\frac{6Q}{4Q+\lambda}\Omega_{G_3} \leq 7 \times 10^{-5}. \tag{4.43}$$

This is a sufficient condition, so the actual upper bound on Ω_{G_3} is slightly tighter. Unlike the case discussed in Sec. IV A, the coupling Q is not particularly bounded from above. Indeed, the numerical simulation of Fig. 5 corresponds to $Q = 0.1$, but the LLR bound is satisfied. This property comes from the fact that the cubic Galileon term suppresses the field kinetic energy through the cosmological Vainshtein screening, so that the variable x in $\alpha_{\rm M} = -2\sqrt{6}Qx$ is restricted to be small. We note that, even though $\Omega_K \ll \Omega_{G_3}$, Ω_{G_3} is much smaller than Ω_V, so the cubic Galileon is subdominant as the dark energy density.

The asymptotic value of ϵ_ϕ in the future is close to $h(\simeq 0)$ to realize $x' = 0$ with $x \neq 0$ in Eq. (3.17). Then, the scalar propagation speed squared should approach the value $c_s^2 \simeq (2 + \epsilon_\phi)/3 \simeq 2/3$, which is indeed the case for the numerical simulation in Fig. 6. Since the condition $c_s^2 > 0$ is satisfied from the radiation dominance to the future, there is no Laplacian instability of scalar perturbations.

The numerical simulation of Fig. 6 corresponds to $\lambda = 1$, but $w_{\rm DE}$ is very close to -1 even in the asymptotic future. This behavior is different from case (D) in Fig. 4 where the solutions finally reach the fixed point (b) with the large deviation of $w_{\rm DE}$ from -1. In the screened cosmology discussed in this section, the future asymptotic solution is characterized by Eqs. (4.41) and (4.42) with the strongly suppressed kinetic energy ($\Omega_K \ll \Omega_{G_3} \ll \Omega_V \simeq 1$). In this case, the dark energy equation of state is given by Eq. (4.25) with $h \simeq 0$ in the asymptotic future and hence $w_{\rm DE} \simeq -1$.

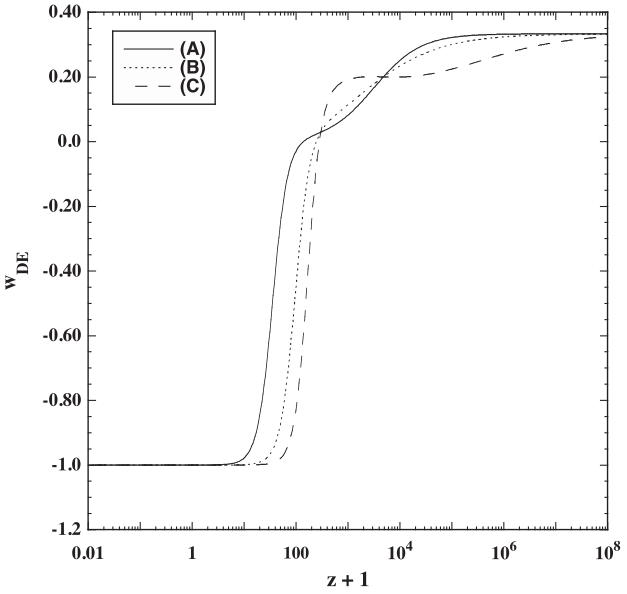

FIG. 7. Evolution of $w_{\rm DE}$ versus $z + 1$ for $\lambda = 2$ for the same initial conditions of x, Ω_V, Ω_{G_3}, Ω_r, and y as those used in Fig. 5. Each case corresponds to (A) $Q = 0.153$, (B) $Q = 0.010$, and (C) $Q = 0.001$.

Since the cosmological Vainshtein screening for the field kinetic energy efficiently works for $\beta_3 \gg 1$, it is possible to realize $w_{\rm DE}$ close to -1 at low redshifts even for $\lambda > \sqrt{2}$. In Fig. 7, we plot the evolution of $w_{\rm DE}$ for $\lambda = 2$ with three different values of Q, all of which correspond to $\beta_3 \simeq 1.0 \times 10^7$. Even with λ larger than $\sqrt{2}$, $w_{\rm DE}$ is very close to -1 from the redshift $z \approx \mathcal{O}(10)$ toward the asymptotic future. For decreasing Q, the deviation of $F = e^{-2Q(\phi-\phi_0)/M_{\rm pl}}$ from 1 tends to be smaller in the past, and hence the solutions enter the regime $\Omega_V F > 1 - F$ at an earlier time. Then, from Eq. (4.25), the approach of $w_{\rm DE}$ to -1 occurs at higher redshifts. In case (A) of Fig. 7 we have $\alpha_{\rm M}(t_0) = 6.98 \times 10^{-5}$, so this is close to the LLR upper limit (2.18). For decreasing Q with given values of β_3 and λ, $\alpha_{\rm M}(t_0)$ gets smaller, e.g., $\alpha_{\rm M}(t_0) = 3.87 \times 10^{-6}$ and $\alpha_{\rm M}(t_0) = 3.82 \times 10^{-7}$ in cases (B) and (C) of Fig. 7, respectively. For smaller $\alpha_{\rm M}(t_0)$, the models mimic the ΛCDM behavior ($w_{\rm DE} = -1$) from earlier cosmological epochs to today.

V. MODIFIED GRAVITATIONAL WAVE PROPAGATION

In this section, we study the modified GW propagation induced by the nonminimal coupling $F(\phi)R$ and compute the difference between GW and luminosity distances for the

dark energy cosmology discussed in Sec. IV. The perturbed line element containing tensor perturbations h_{ij} on the flat FLRW background is given by

$$ds^2 = -dt^2 + a^2(t)(\delta_{ij} + h_{ij})dx^i dx^j. \tag{5.1}$$

To satisfy the transverse and traceless conditions $\partial^j h_{ij} = 0$ and $h_i{}^i = 0$, we choose the nonvanishing components of h_{ij}, as $h_{11} = h_1(t,z)$, $h_{22} = -h_1(t,z)$, and $h_{12} = h_{21} = h_2(t,z)$. Expanding the action (2.1) up to quadratic order in h_{ij} and integrating it by parts, the resulting second-order action of tensor perturbations yields [7,80,98]

$$\mathcal{S}_t^{(2)} = \int dt d^3x \sum_{i=1}^{2} \frac{M_{\rm pl}^2}{4} F(\phi) a^3 \left[\dot{h}_i^2 - \frac{1}{a^2}(\partial h_i)^2 \right]. \tag{5.2}$$

In general, the speed c_t of tensor perturbations appears as the spatial derivative term $-(c_t^2/a^2)(\partial h_i)^2$ in the square bracket of Eq. (5.2). In our theory c_t^2 is equivalent to 1, so it automatically satisfies the observational bound of GW propagation speed [14].

In Fourier space with the coming wave number k, the two polarization modes h_i (where $i = 1, 2$) obey the wave equation,

$$\ddot{h}_i + H(3 + \alpha_{\rm M})\dot{h}_i + \frac{k^2}{a^2} h_i = 0. \tag{5.3}$$

By defining

$$\hat{h}_i \equiv a_{\rm GW} h_i, \qquad a_{\rm GW} \equiv \sqrt{F} a, \tag{5.4}$$

Eq. (5.3) can be expressed in the form

$$\frac{d^2 \hat{h}_i}{d\eta^2} + \left(k^2 - \frac{1}{a_{\rm GW}} \frac{d^2 a_{\rm GW}}{d\eta^2} \right) \hat{h}_i = 0, \tag{5.5}$$

where $\eta = \int a^{-1} dt$ is the conformal time.

For the physical wavelength much smaller than the Hubble radius ($k/a \gg H$), the second term in the parenthesis of Eq. (5.5) can be ignored relative to k^2. Then, the solution to Eq. (5.5) is simply given by a plane wave with a constant amplitude ($\hat{h}_i \simeq e^{\pm ik\eta}$). The amplitude of $h_i = \hat{h}_i/a_{\rm GW}$ decreases in proportion to $1/a_{\rm GW}$. The GW produced by a binary inspiral (point particles with two masses m_1 and m_2) at redshift z with the comoving distance r from an observer has the amplitude [99]

$$h_A(z) = \frac{4}{a(t_s) r} \left(\frac{G_{\rm N}(t_s) M_c}{c^2} \right)^{5/3} \left(\frac{\pi f_s}{c} \right)^{2/3}, \tag{5.6}$$

where t_s is the time at emission, $G_{\rm N}(t_s) = G/F(t_s)$ is the screened gravitational coupling at $t = t_s$ with $G = 1/(8\pi M_{\rm pl}^2)$, $M_c = (m_1 m_2)^{3/5}/(m_1 + m_2)^{1/5}$ is the chirp mass, and f_s is the frequency measured by the clock of source. We note that the speed of light c is explicitly written in Eq. (5.6). Today's GW amplitude $h_A(0)$ observed at time t_0 is related to $h_A(z)$, as $h_A(0) = [a_{\rm GW}(t_s)/a_{\rm GW}(t_0)] h_A(z)$. On using the property $a_{\rm GW}(t_0) = a(t_0)$, it follows that

$$h_A(0) = \frac{a_{\rm GW}(t_s)}{a(t_s)} \frac{1}{F(t_s)^{5/3}} h_{A,{\rm GR}}(0), \tag{5.7}$$

where

$$h_{A,{\rm GR}}(0) = \frac{4}{a(t_0) r} \left(\frac{G M_c}{c^2} \right)^{5/3} \left(\frac{\pi f_s}{c} \right)^{2/3} \tag{5.8}$$

is the observed GW amplitude in GR. On the flat FLRW background, the luminosity distance from the observer to the source is given by $d_L(z) = (1+z) a(t_0) r$. By using $d_L(z)$ and the observed GW frequency $f_{\rm obs} = f_s/(1+z)$, one can write Eq. (5.8) in the form

$$h_{A,{\rm GR}}(0) = \frac{4}{d_L(z)} \left(\frac{G \mathcal{M}_c}{c^2} \right)^{5/3} \left(\frac{\pi f_{\rm obs}}{c} \right)^{2/3}, \tag{5.9}$$

where $\mathcal{M}_c \equiv (1+z) M_c$. Substituting Eq. (5.9) into Eq. (5.7), the observed GW amplitude is expressed as

$$h_A(0) = \frac{4}{d_{\rm GW}(z)} \left(\frac{G_{\rm N}(t_s) \mathcal{M}_c}{c^2} \right)^{5/3} \left(\frac{\pi f_{\rm obs}}{c} \right)^{2/3}, \tag{5.10}$$

where

$$d_{\rm GW}(z) = d_L(z) \frac{a(t_s)}{a_{\rm GW}(t_s)} = \frac{d_L(z)}{\sqrt{F(t_s)}}. \tag{5.11}$$

On using Eq. (2.17), the quantity F at redshift z is generally expressed as

$$F(z) = \exp\left[-\int_0^z \frac{\alpha_{\rm M}(\tilde{z})}{1+\tilde{z}} d\tilde{z} \right]. \tag{5.12}$$

Then, the relative ratio between $d_{\rm GW}(z)$ and $d_L(z)$ yields

$$\frac{d_{\rm GW}(z)}{d_L(z)} = \exp\left[\int_0^z \frac{\alpha_{\rm M}(\tilde{z})}{2(1+\tilde{z})} d\tilde{z} \right]. \tag{5.13}$$

If $\alpha_{\rm M}(z) > 0$, then $d_{\rm GW}(z) > d_L(z)$ for $z > 0$. For positive $\alpha_{\rm M}(z)$, which is the case for our nonminimally coupled dark energy scenario, there is the LLR bound $\alpha_{\rm M}(0) \le \alpha_{\rm max}$, where $\alpha_{\rm max} = 7 \times 10^{-5}$. Provided that the past value of $\alpha_{\rm M}(z)$ is smaller than $\alpha_{\rm M}(0)$, the ratio (5.13) is in the range

$$\frac{d_{\rm GW}(z)}{d_L(z)} \le (1+z)^{\alpha_{\rm max}/2}. \tag{5.14}$$

Expanding the term $(1+z)^{\alpha_{\rm max}/2}$ around $\alpha_{\rm max} = 0$, it follows that

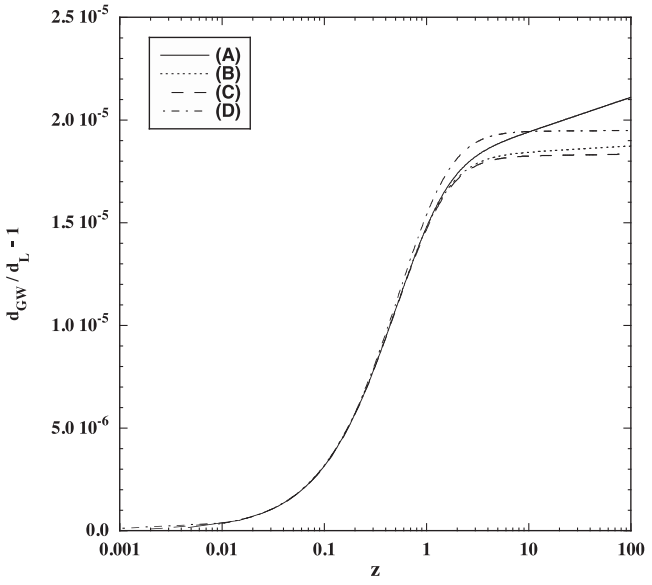

FIG. 8. The relative difference $d_{\rm GW}(z)/d_L(z)-1$ versus z corresponding to the cases (A), (B), (C), and (D) shown in Fig. 4.

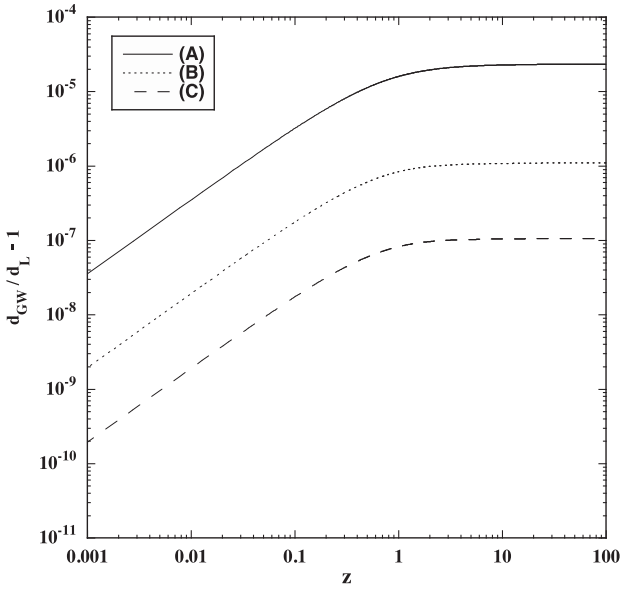

FIG. 9. The relative difference $d_{\rm GW}(z)/d_L(z)-1$ versus z corresponding to the cases (A), (B), and (C) shown in Fig. 7.

$$\mu_d(z) \equiv \frac{d_{\rm GW}(z)}{d_L(z)} - 1 \lesssim \frac{\alpha_{\rm max}}{2}\ln(1+z), \qquad (5.15)$$

where we ignored the terms higher than the order $\alpha_{\rm max}$. Substituting $\alpha_{\rm max} = 7\times 10^{-5}$ into the right-hand side of Eq. (5.15), we have $(\alpha_{\rm max}/2)\ln(1+z) = 1.6\times 10^{-4}$ at $z = 100$. Then, the quantity $\mu_d(z)$ is constrained to be

$$\mu_d(z) \lesssim 10^{-4} \quad (\text{for } 0 < z < 100). \qquad (5.16)$$

This is the maximum allowed difference between $d_{\rm GW}(z)$ and $d_L(z)$ constrained from the LLR data.

For concreteness, let us consider the nonminimally coupled dark energy scenario given by the action (2.1). From Eq. (5.11), we have

$$\frac{d_{\rm GW}(z)}{d_L(z)} = e^{Q[\phi(z)-\phi_0]/M_{\rm pl}}. \qquad (5.17)$$

The change of ϕ from the redshift z to today leads to the difference between $d_{\rm GW}(z)$ and $d_L(z)$. As we studied in Sec. IV, there are two qualitative different cases: (i) $|\beta_3| \ll 1$ with the ϕMDE, and (ii) $|\beta_3| \gg 1$ without the ϕMDE.

In case (i), the LLR data place the tight upper limit (4.27) on the coupling constant Q. In Fig. 8, we plot $\mu_d(z) = d_{\rm GW}(z)/d_L(z) - 1$ in the redshift range $0 < z < 100$ for four different combinations of Q and λ. Each plot corresponds to cases (A), (B), (C), and (D) shown in Fig. 4. In all these cases, the LLR bound is marginally satisfied, i.e., $\alpha_{\rm M}(0) \simeq 7\times 10^{-5}$. For the redshift $z < 1$, the values of $\mu_d(z)$ are similar to each other among the four cases, with $\mu_d \simeq 1.5\times 10^{-5}$ at $z = 1$. The difference starts to appear for $z > 1$, but the orders of $\mu_d(z)$ at $z = 100$ are still 10^{-5}. As we estimated in Eq. (4.15), the value of $\alpha_{\rm M}$ during the ϕMDE is of order $4Q^2$, and hence $\alpha_{\rm M}^{(a)} \le 4.6\times 10^{-5}$ under the bound (4.27). Since $\alpha_{\rm M}^{(a)}$ is smaller than today's value $\alpha_{\rm M}(0)$, the main contribution to the ratio (5.13) comes from $\alpha_{\rm M}(z)$ at low redshifts. Since $\alpha_{\rm M}(z)$ at $z \le 1$ is not much different from today's value $\alpha_{\rm M}(0) \simeq 7\times 10^{-5}$ in the numerical simulation of Fig. 8, the maximum value of μ_d for $z \gg 1$ can be estimated by substituting $z = 1$ into Eq. (5.15), i.e., $\mu_d \lesssim \mathcal{O}(10^{-5})$. Indeed, this crude estimation is consistent with the numerical values of μ_d at $z \gg 1$ in Fig. 8. If $\alpha_{\rm M}(0)$ is smaller than 7×10^{-5}, the resulting values of μ_d at high redshifts are less than the order 10^{-5}.

In case (ii), the upper limit of Q is not particularly constrained from the LLR experiment, but the cosmological Vainshtein screening leads to the strong suppression of $\dot\phi$. The case (A) in Fig. 9, which corresponds to $Q = 0.153$ and $\lambda = 2$, is marginally within the LLR bound. In this case, the value of $\alpha_{\rm M}$ for $z \gg 1$ is of order 10^{-5}. As we see in Fig. 5, $\alpha_{\rm M}$ rapidly decreases toward the asymptotic past, and hence the main contribution to $\mu_d(z)$ again comes from $\alpha_{\rm M}(z)$ at $z \le \mathcal{O}(1)$. In cases (B) and (C) of Fig. 9, which correspond to the couplings $Q = 0.01$ and $Q = 0.001$, today's values of $\alpha_{\rm M}$ are smaller than that in case (A) by 1 and 2 orders of magnitude, respectively. In cases (B) and (C), the numerical values of $\mu_d(z)$ at $z = 100$ are 1.1×10^{-6} and 1.1×10^{-7}, respectively, so the order difference of $\alpha_{\rm M}(0)$ directly affects μ_d at high redshifts.

From the above discussion, we have $\mu_d(z) \le \mathcal{O}(10^{-5})$ for $0 < z < 100$ in both unscreened and screened cosmological backgrounds. This property is mostly attributed to the fact that the value of $\alpha_{\rm M}$ at low redshifts is tightly limited by the LLR bound. Unless the ratio $d_{\rm GW}(z)/d_L(z)$

is measured in high accuracy, it is challenging to observationally distinguish nonminimally coupled theories from minimally coupled theories.

VI. CONCLUSIONS

We studied how the recent LLR measurement constrains nonminimally coupled dark energy models given by the action (2.1). The existence of nonminimal coupling of the form $F(\phi)R$, where $F(\phi)=e^{-2Q(\phi-\phi_0)/M_{\rm pl}}$, gives rise to the propagation of fifth forces characterized by the coupling constant Q with nonrelativistic matter. For a massless scalar field without derivative interactions, the coupling is constrained to be in the range $|Q|\le 2.4\times 10^{-3}$ from the Cassini experiment. The cubic Galileon coupling $\beta_3 M^{-3}X\Box\phi$ allows one to recover the Newtonian behavior in overdensity regions even for $|Q|>2.4\times 10^{-3}$. Since the late-time dominance of Galileons as the dark energy density generally leads to the incompatibility with observations, we considered the potential $V(\phi)$ of a light scalar field.

In local regions of the Universe, the Galileon self-interaction screens fifth forces within the Vainshtein radius (2.8). The Vainshtein mechanism is at work within the solar system for the cubic coupling in the range $|\beta_3 Q|\gg 10^{-17}$. In spite of the screened scalar-matter interaction, the time variation of ϕ associated with the dynamics of dark energy survives in the expression of gravitational coupling $G_{\rm N}$ in overdensity regions, with the form $G_{\rm N}=1/[8\pi M_{\rm pl}^2F(\phi)]$. The recent LLR data placed the tight constraint (2.15) on the time variation of $G_{\rm N}$, which translates to the bound (2.18) on today's value of $\alpha_{\rm M}=\dot{F}/(HF)$.

To investigate the evolution of $\alpha_{\rm M}$ as well as field density parameters Ω_K, Ω_V, and Ω_{G_3}, we expressed dynamical equations of motion on the flat FLRW background in the autonomous form given by (3.17)–(3.20). In addition to the dark energy equation of state $w_{\rm DE}$, we also considered the quantities q_s and c_s^2 to ensure the absence of ghosts and Laplacian instabilities. Together with Eq. (3.22), the dynamical background equations of motion can be applied to any scalar potential $V(\phi)$.

In Sec. IV, we studied the cosmological dynamics in details for the exponential potential (4.1). For the cubic coupling satisfying the condition (2.12), Ω_{G_3} can dominate over Ω_K in the radiation-dominated epoch. We showed that, under the conditions $|\alpha_{\rm M}|\gg\Omega_{G_3}$ and $|\alpha_{\rm M}|\ll\Omega_{G_3}$, the field density parameters and $|\alpha_{\rm M}|$ evolve as Eqs. (4.7) and (4.8), respectively, during the radiation era. After the onset of matter dominance, there are two qualitatively different cases: (i) unscreened cosmology with $|\beta_3|\ll 1$, and (ii) screened cosmology with $|\beta_3|\gg 1$.

In case (i), there is the kinetically driven ϕMDE in which $\alpha_{\rm M}$ is given by $\alpha_{\rm M}^{(a)}=4Q^2/(1-2Q^2)$. The solutions finally approach the fixed point (b) with cosmic acceleration at which $\alpha_{\rm M}$ is equivalent to $\alpha_{\rm M}^{(b)}=2Q(\lambda+4Q)/(1-Q\lambda-4Q^2)$. For positive λ and Q the inequality $\alpha_{\rm M}^{(b)}>\alpha_{\rm M}^{(a)}>0$ holds, so the necessary condition for consistency with the LLR bound (2.18) corresponds to $\alpha_{\rm M}^{(a)}\le 7\times 10^{-5}$, i.e., $Q\le 4.2\times 10^{-3}$. Applying today's bound $\alpha_{\rm M}(t_0)\le 7\times 10^{-5}$ to case (i), the coupling is constrained to be $Q\le 3.4\times 10^{-3}$ in the limit $\lambda\to 0$. As we see in Fig. 3, for increasing λ, the upper bound on Q is tighter than the bound $Q\le 3.4\times 10^{-3}$. We also showed that $w_{\rm DE}$ temporally approaches the value close to -1 during the matter era after the dominance of the term $\Omega_V F$ over $1-F$. For larger λ, the deviation of $w_{\rm DE}$ from -1 on the attractor point (b) tends to be larger; see Fig. 4.

In case (ii), the cosmological Vainshtein screening of field kinetic energy is at work, so the condition $\Omega_K\ll\Omega_{G_3}$ is satisfied even after the end of radiation dominance. As we observe in Fig. 5, $\alpha_{\rm M}$ grows during the matter era and finally approaches a constant related to Ω_{G_3}, as $\alpha_{\rm M}=6Q\Omega_{G_3}/(4Q+\lambda)$. Provided that this asymptotic value of $\alpha_{\rm M}$ is smaller than the order 10^{-4}, the case (ii) can be consistent with today's LLR bound (2.18). Since Ω_{G_3} is much smaller than Ω_V today, the coupling Q is not particularly bounded from above. The field kinetic energy is strongly suppressed by the cosmological Vainshtein screening, i.e., $\Omega_K\ll\Omega_{G_3}\ll\Omega_V$, so it is possible to realize $w_{\rm DE}$ very close to -1 at low redshifts even for $\lambda>\sqrt{2}$; see Fig. 7. This behavior is different from that in case (i) where $w_{\rm DE}$ deviates from -1 in the asymptotic future for increasing λ in the range $\lambda<\sqrt{2}$.

In Sec. V, we derived the relation between the GW and luminosity distances in the form (5.11). In terms of the parameter $\alpha_{\rm M}$, the ratio between $d_{\rm GW}(z)$ and $d_L(z)$ is given by Eq. (5.13). Provided that $\alpha_{\rm M}(z)$ in the past is smaller than today's value $\alpha_{\rm M}(0)$, the LLR experiment gives the upper limit on the relative difference $\mu_d(z)=d_{\rm GW}(z)/d_L(z)-1$ as Eq. (5.15). We computed the quantity $\mu_d(z)$ for the nonminimally coupled dark energy scenario discussed in Sec. IV and showed that $\mu_d(z)$ for $z\ge\mathcal{O}(1)$ is mostly determined by today's value of $\alpha_{\rm M}$. For $\alpha_{\rm M}(0)$ close to the LLR upper limit 7×10^{-5}, $\mu_d(z)$ is of order 10^{-5} in the redshift range $1<z<100$. This property is independent of the unscreened and screened cosmological backgrounds, so the LLR constraint gives a tight restriction on the deviation of $d_{\rm GW}(z)$ from $d_L(z)$ in nonminimally coupled theories.

In this paper we did not study the evolution of scalar cosmological perturbations relevant to the observations of large-scale structures and weak lensing, but it is straightforward to do so by using the linear perturbation equations of motion derived in Refs. [7,80,100]. In the unscreened cosmological background the upper limit of Q is tightly constrained from the LLR experiment, so the effective gravitational couplings felt by matter and light are close to $G_{\rm N}$ [80]. In the screened background not only Ω_K but also Ω_{G_3} is generally much smaller than 1 at low redshifts, so it is expected that the gravitational interaction is not substantially modified from that in GR. At the background

level, the dark energy equations of state in the unscreened and screened cases exhibit some difference especially in the late cosmological epoch. It will be of interest to place further constraints on the allowed parameter space of our theory by exploiting the observational data of cosmic expansion and growth histories.

ACKNOWLEDGMENTS

The author thanks Michele Maggiore for useful discussions. The author is supported by the Grant-in-Aid for Scientific Research Fund of the JSPS No. 16K05359 and MEXT KAKENHI Grant-in-Aid for Scientific Research on Innovative Areas "Cosmic Acceleration" (No. 15H05890).

[1] A. G. Riess *et al.*, Astron. J. **116**, 1009 (1998).
[2] S. Perlmutter *et al.*, Astrophys. J. **517**, 565 (1999).
[3] Y. Fujii, Phys. Rev. D **26**, 2580 (1982); L. H. Ford, Phys. Rev. D **35**, 2339 (1987); C. Wetterich, Nucl. Phys. **B302**, 668 (1988); T. Chiba, N. Sugiyama, and T. Nakamura, Mon. Not. R. Astron. Soc. **289**, L5 (1997); P. G. Ferreira and M. Joyce, Phys. Rev. Lett. **79**, 4740 (1997); R. R. Caldwell, R. Dave, and P. J. Steinhardt, Phys. Rev. Lett. **80**, 1582 (1998).
[4] C. Armendariz-Picon, T. Damour, and V. F. Mukhanov, Phys. Lett. B **458**, 209 (1999); T. Chiba, T. Okabe, and M. Yamaguchi, Phys. Rev. D **62**, 023511 (2000); C. Armendariz-Picon, V. F. Mukhanov, and P. J. Steinhardt, Phys. Rev. Lett. **85**, 4438 (2000).
[5] G. W. Horndeski, Int. J. Theor. Phys. **10**, 363 (1974).
[6] C. Deffayet, X. Gao, D. A. Steer, and G. Zahariade, Phys. Rev. D **84**, 064039 (2011).
[7] T. Kobayashi, M. Yamaguchi, and J. Yokoyama, Prog. Theor. Phys. **126**, 511 (2011).
[8] C. Charmousis, E. J. Copeland, A. Padilla, and P. M. Saffin, Phys. Rev. Lett. **108**, 051101 (2012).
[9] G. D. Moore and A. E. Nelson, J. High Energy Phys. 09 (2001) 023.
[10] R. Kimura and K. Yamamoto, J. Cosmol. Astropart. Phys. 07 (2012) 050.
[11] B. P. Abbott *et al.* (LIGO Scientific and Virgo Collaborations), Phys. Rev. Lett. **116**, 061102 (2016).
[12] L. Lombriser and A. Taylor, J. Cosmol. Astropart. Phys. 03 (2016) 031.
[13] J. Beltran Jimenez, F. Piazza, and H. Velten, Phys. Rev. Lett. **116**, 061101 (2016).
[14] B. P. Abbott *et al.* (LIGO Scientific and Virgo Collaborations), Phys. Rev. Lett. **119**, 161101 (2017).
[15] A. Goldstein *et al.*, Astrophys. J. **848**, L14 (2017).
[16] P. Creminelli and F. Vernizzi, Phys. Rev. Lett. **119**, 251302 (2017).
[17] J. M. Ezquiaga and M. Zumalacarregui, Phys. Rev. Lett. **119**, 251304 (2017).
[18] J. Sakstein and B. Jain, Phys. Rev. Lett. **119**, 251303 (2017).
[19] T. Baker, E. Bellini, P. G. Ferreira, M. Lagos, J. Noller, and I. Sawicki, Phys. Rev. Lett. **119**, 251301 (2017).
[20] L. Amendola, M. Kunz, I. D. Saltas, and I. Sawicki, Phys. Rev. Lett. **120**, 131101 (2018).
[21] A. Nicolis, R. Rattazzi, and E. Trincherini, Phys. Rev. D **79**, 064036 (2009).
[22] C. Deffayet, G. Esposito-Farese, and A. Vikman, Phys. Rev. D **79**, 084003 (2009).
[23] C. Deffayet, S. Deser, and G. Esposito-Farese, Phys. Rev. D **80**, 064015 (2009).
[24] C. Deffayet, O. Pujolas, I. Sawicki, and A. Vikman, J. Cosmol. Astropart. Phys. 10 (2010) 026.
[25] C. Brans and R. H. Dicke, Phys. Rev. **124**, 925 (1961).
[26] P. G. Bergmann, Int. J. Theor. Phys. **1**, 25 (1968).
[27] T. V. Ruzmaikina and A. A. Ruzmaikin, Zh. Eksp. Teor. Fiz. **57**, 680 (1969).
[28] A. A. Starobinsky, Phys. Lett. B **91**, 99 (1980).
[29] T. Damour and K. Nordtvedt, Phys. Rev. D **48**, 3436 (1993).
[30] T. Damour and A. M. Polyakov, Nucl. Phys. **B423**, 532 (1994).
[31] L. Amendola, Phys. Rev. D **60**, 043501 (1999).
[32] J. P. Uzan, Phys. Rev. D **59**, 123510 (1999).
[33] T. Chiba, Phys. Rev. D **60**, 083508 (1999).
[34] N. Bartolo and M. Pietroni, Phys. Rev. D **61**, 023518 (1999).
[35] F. Perrotta, C. Baccigalupi, and S. Matarrese, Phys. Rev. D **61**, 023507 (1999).
[36] B. Boisseau, G. Esposito-Farese, D. Polarski, and A. A. Starobinsky, Phys. Rev. Lett. **85**, 2236 (2000).
[37] G. Esposito-Farese and D. Polarski, Phys. Rev. D **63**, 063504 (2001).
[38] S. Tsujikawa, K. Uddin, S. Mizuno, R. Tavakol, and J. Yokoyama, Phys. Rev. D **77**, 103009 (2008).
[39] A. De Felice and S. Tsujikawa, Living Rev. Relativity **13**, 3 (2010).
[40] K. Nordtvedt, Astrophys. J. **161**, 1059 (1970).
[41] C. M. Will, Astrophys. J. **163**, 611 (1971).
[42] C. M. Will, Living Rev. Relativity **9**, 3 (2006).
[43] C. M. Will, Living Rev. Relativity **17**, 4 (2014).
[44] J. Khoury and A. Weltman, Phys. Rev. Lett. **93**, 171104 (2004).
[45] J. Khoury and A. Weltman, Phys. Rev. D **69**, 044026 (2004).
[46] L. Amendola, D. Polarski, and S. Tsujikawa, Phys. Rev. Lett. **98**, 131302 (2007).
[47] W. Hu and I. Sawicki, Phys. Rev. D **76**, 064004 (2007).
[48] A. A. Starobinsky, JETP Lett. **86**, 157 (2007).
[49] S. A. Appleby and R. A. Battye, Phys. Lett. B **654**, 7 (2007).
[50] S. Tsujikawa, Phys. Rev. D **77**, 023507 (2008).
[51] A. V. Frolov, Phys. Rev. Lett. **101**, 061103 (2008).
[52] S. Tsujikawa, Phys. Rev. D **76**, 023514 (2007).
[53] S. Tsujikawa, R. Gannouji, B. Moraes, and D. Polarski, Phys. Rev. D **80**, 084044 (2009).

[54] L. Lombriser, A. Slosar, U. Seljak, and W. Hu, Phys. Rev. D **85**, 124038 (2012).
[55] R. A. Battye, B. Bolliet, and F. Pace, Phys. Rev. D **97**, 104070 (2018).
[56] A. I. Vainshtein, Phys. Lett. B **39**, 393 (1972).
[57] C. Deffayet, G. R. Dvali, G. Gabadadze, and A. I. Vainshtein, Phys. Rev. D **65**, 044026 (2002).
[58] M. A. Luty, M. Porrati, and R. Rattazzi, J. High Energy Phys. 09 (2003) 029.
[59] E. Babichev, C. Deffayet, and R. Ziour, J. High Energy Phys. 05 (2009) 098.
[60] C. Burrage and D. Seery, J. Cosmol. Astropart. Phys. 08 (2010) 011.
[61] P. Brax, C. Burrage, and A. C. Davis, J. Cosmol. Astropart. Phys. 09 (2011) 020.
[62] E. Babichev, C. Deffayet, and G. Esposito-Farese, Phys. Rev. Lett. **107**, 251102 (2011).
[63] A. De Felice, R. Kase, and S. Tsujikawa, Phys. Rev. D **85**, 044059 (2012).
[64] R. Kimura, T. Kobayashi, and K. Yamamoto, Phys. Rev. D **85**, 024023 (2012).
[65] R. Kase and S. Tsujikawa, J. Cosmol. Astropart. Phys. 08 (2013) 054.
[66] A. De Felice and S. Tsujikawa, Phys. Rev. Lett. **105**, 111301 (2010).
[67] A. De Felice and S. Tsujikawa, Phys. Rev. D **84**, 124029 (2011).
[68] R. Gannouji and M. Sami, Phys. Rev. D **82**, 024011 (2010).
[69] A. Ali, R. Gannouji, and M. Sami, Phys. Rev. D **82**, 103015 (2010).
[70] S. Nesseris, A. De Felice, and S. Tsujikawa, Phys. Rev. D **82**, 124054 (2010).
[71] S. A. Appleby and E. V. Linder, J. Cosmol. Astropart. Phys. 08 (2012) 026.
[72] J. Neveu, V. Ruhlmann-Kleider, A. Conley, N. Palanque-Delabrouille, P. Astier, J. Guy, and E. Babichev, Astron. Astrophys. **555**, A53 (2013).
[73] A. Barreira, B. Li, A. Sanchez, C. M. Baugh, and S. Pascoli, Phys. Rev. D **87**, 103511 (2013).
[74] A. Barreira, B. Li, C. Baugh, and S. Pascoli, J. Cosmol. Astropart. Phys. 08 (2014) 059.
[75] J. Renk, M. Zumalacaregui, F. Montanari, and A. Barreira, J. Cosmol. Astropart. Phys. 10 (2017) 020.
[76] S. Peirone, N. Frusciante, B. Hu, M. Raveri, and A. Silvestri, Phys. Rev. D **97**, 063518 (2018).
[77] A. Ali, R. Gannouji, M. W. Hossain, and M. Sami, Phys. Lett. B **718**, 5 (2012).
[78] R. Kase, S. Tsujikawa, and A. De Felice, Phys. Rev. D **93**, 024007 (2016).
[79] J. G. Williams, S. G. Turyshev, and D. H. Boggs, Phys. Rev. Lett. **93**, 261101 (2004).
[80] R. Kase and S. Tsujikawa, Int. J. Mod. Phys. D **28**, 1942005 (2019).
[81] F. Hofmann and J. Muller, Classical Quantum Gravity **35**, 035015 (2018).
[82] E. Belgacem, A. Finke, A. Frassino, and M. Maggiore, J. Cosmol. Astropart. Phys. 02 (2019) 035.
[83] L. Amendola, Phys. Rev. D **62**, 043511 (2000).
[84] I. D. Saltas, I. Sawicki, L. Amendola, and M. Kunz, Phys. Rev. Lett. **113**, 191101 (2014).
[85] A. Nishizawa, Phys. Rev. D **97**, 104037 (2018).
[86] S. Arai and A. Nishizawa, Phys. Rev. D **97**, 104038 (2018).
[87] E. Belgacem, Y. Dirian, S. Foffa, and M. Maggiore, Phys. Rev. D **97**, 104066 (2018).
[88] L. Amendola, I. Sawicki, M. Kunz, and I. D. Saltas, J. Cosmol. Astropart. Phys. 08 (2018) 030.
[89] W. Zhao, B. S. Wright, and B. Li, J. Cosmol. Astropart. Phys. 10 (2018) 052.
[90] E. Belgacem, Y. Dirian, S. Foffa, and M. Maggiore, Phys. Rev. D **98**, 023510 (2018).
[91] J. M. Ezquiaga and M. Zumalacarregui, Front. Astron. Space Sci. **5**, 44 (2018).
[92] M. Lagos, M. Fishbach, P. Landry, and D. E. Holz, arXiv: 1901.03321.
[93] S. Nesseris and S. Tsujikawa, Phys. Rev. D **90**, 024070 (2014).
[94] C. de Rham and S. Melville, Phys. Rev. Lett. **121**, 221101 (2018).
[95] E. J. Copeland, A. R. Liddle, and D. Wands, Phys. Rev. D **57**, 4686 (1998).
[96] E. J. Copeland, M. Sami, and S. Tsujikawa, Int. J. Mod. Phys. D **15**, 1753 (2006).
[97] E. Bellini and I. Sawicki, J. Cosmol. Astropart. Phys. 07 (2014) 050.
[98] A. De Felice and S. Tsujikawa, J. Cosmol. Astropart. Phys. 02 (2012) 007.
[99] M. Maggiore, *Gravitational Waves: Theory and Experiments* (Oxford University Press, Oxford, 2007), Vol. 1.
[100] A. De Felice, T. Kobayashi, and S. Tsujikawa, Phys. Lett. B **706**, 123 (2011).